Science of the Total Environment 989 (2025) 179880

Contents lists available at ScienceDirect

Science of the Total Environment

journal homepage: www.elsevier.com/locate/scitotenv

Comparing machine learning isoscapes of $^{87}Sr/^{86}Sr$ ratios of plants on the island of Sardinia: Implications for the use of isoscapes for assessing the provenance of biological specimens

Emily Holt [a,*], Federico Lugli [b,c], Davide Schirru [d], Melania Gigante [e], Katie Faillace [a], Marc-Alban Millet [a], Morten Andersen [a], Richard Madgwick [a]

[a] School of History, Archaeology and Religion, Cardiff University, John Percival Building, Colum Drive, Cardiff CF10 3EU, United Kingdom
[b] Institut für Geowissenschaften, Goethe University Frankfurt, Altenhöferallee 1, Frankfurt am Main 60438, Germany
[c] Department of Chemical and Geological Sciences, University of Modena and Reggio Emilia, Via Giuseppe Campi 103, Modena 41125, Italy
[d] Dipartimento di Scienze dell'Antichità, Università degli Studi di Roma "La Sapienza", Via dei Volsci 122, 00185 Roma, Italy
[e] Department of Cultural Heritage, University of Padua, Piazza Capitaniato 7, 35139 Padova, Italy

HIGHLIGHTS

- The accuracy of isoscapes, including machine learning isoscapes, cannot be assumed
- Increasing data points showed diminishing returns in improving isoscape accuracy
- Low root mean squared error did not indicate isoscape accuracy for new data points
- The generalizability of strontium isoscapes across archives requires further research
- Isoscapes should be validated before they are used for interpretation

GRAPHICAL ABSTRACT

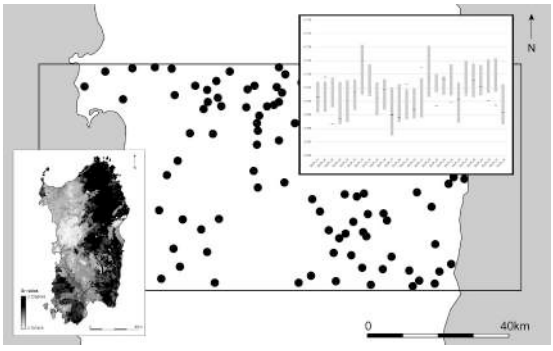

ARTICLE INFO

Editor: Bo Gao

Keywords:
Strontium isotopes
Isoscapes
Machine Learning
Provenance studies
Biosphere
Mediterranean isotopic landscapes

ABSTRACT

Strontium isotope analysis is widely used to evaluate the provenance and mobility of biological specimens. Frequently applied in archaeology, palaeontology, ecology, forensics, and food science, strontium isotope analysis compares the $^{87}Sr/^{86}Sr$ ratio of a specimen against a strontium isoscape – a representation of expected $^{87}Sr/^{86}Sr$ ratios across a landscape – to identify areas that are more and/or less likely to be the source of the specimen. Strontium isoscapes are built using different methods, but all approaches start with empirical $^{87}Sr/^{86}Sr$ ratios sampled from areas with known coordinates and use them to assign likely $^{87}Sr/^{86}Sr$ ratios to unknown areas. Following the publication of Bataille et al., 2018 and Bataille et al., 2020, machine learning using a random forest algorithm has become a common method of producing strontium isoscapes. Despite the recognition that this method requires training with local ratios, especially in geologically complex regions, very little work has evaluated machine learning isoscapes' accuracy. This study compares and evaluates two previously published machine learning isoscapes of Sardinia against new empirical data provided by the project ZANBA.

* Corresponding author.
E-mail address: HoltE@cardiff.ac.uk (E. Holt).

https://doi.org/10.1016/j.scitotenv.2025.179880
Received 8 June 2024; Received in revised form 8 June 2025; Accepted 8 June 2025
Available online 14 June 2025

The ZANBA data is then used to create a third machine learning map of Sardinia, which is tested against previously published empirical data. The three isoscapes show different levels of predictive accuracy, with more primary data points leading to more correct predictions. However, a densely sampled landscape did not create an isoscape that gave substantially more accurate predictions than a moderately densely sampled landscape when tested against primary data from outside the original sampling areas. Areas of an isoscape with low root mean squared error (RMSE), which is often interpreted as indicating accuracy, did not necessarily give more correct predictions. Finally, a machine learning isoscape of Sardinia that incorporates both new and previously published empirical data is presented.

1. Introduction

Strontium isotope analysis is widely used to understand locations of origin and patterns of mobility in archaeology, palaeontology, ecology, forensics, food studies, and other disciplines. Interpreting the results of strontium (Sr) isotope analysis of biological specimens requires comparing analyzed ratios against a baseline map or isoscape, a representation of expected bioavailable $^{87}Sr/^{86}Sr$ ratios across a geographical area. Bioavailable Sr refers to the Sr that can be taken up from bedrocks, sediments, and dusts by living organisms and incorporated into their tissues. For many applications, mapping the bioavailable Sr of plants, animals, and humans is most relevant; this bioavailable Sr comes primarily from sediments and waters. However, for some applications, it may be relevant to consider the bioavailable Sr of organisms that can take Sr more directly from rocks and dust.

Isotopic baseline maps and isoscapes are created using three main methods: domain mapping, contour mapping, and machine learning (ML, see (Holt et al., 2021) for a review of these methods). While each of these methods has advantages and disadvantages, an important advantage of contour mapping and ML is their ability to produce an isoscape for a large area based on a small number of directly analyzed samples. Undertaking isotopic analysis of primary samples is time consuming and can be logistically challenging, while processing a large number of samples may be prohibitively expensive. For these reasons, contour mapping and – increasingly – ML have become the preferred methods for producing isoscapes (Janzen et al., 2020; Scaffidi et al., 2020; Serna et al., 2020; Barbarena et al., 2021; Funck et al., 2021; Lazzerini et al., 2021; Reich et al., 2021; Kramer et al., 2022; Käßner et al., 2023; Wang et al., 2023; Tarrant et al., 2024). However, a drawback of using contour mapping and ML isoscapes to interpret the results from additional samples is that it is difficult to assess how accurately an isoscape reflects the actual distributions of isotopic bioavailability in nature without widespread primary analysis, which is precisely what contour mapping and ML isoscapes were developed to avoid. Consequently, studies that empirically assess the predictive performance of ML maps remain rare.

This study addresses this issue using the island of Sardinia as a case study. New, high-density empirical data provided by the project ZANBA: Zooarchaeology of the Nuragic Bronze Age is used to evaluate and compare the predictive accuracy of two previously published ML $^{87}Sr/^{86}Sr$ isoscapes of Sardinia that operate at different scales. These comprise Bataille et al.'s global isoscape (Bataille et al., 2020), which was developed with five primary data points from Sardinia, and Gigante et al.'s isoscape of southern Sardinia (Gigante et al., 2023), which includes 30 primary data points. Next, we use the ZANBA data to build a new ML isoscape for Sardinia. We then test the ZANBA isoscape as well as the Bataille et al. global isoscape using the empirical data from Gigante et al. This assesses the performance of a ML approach to producing isoscapes when different types, numbers, and distributions of primary data points are used to train the model. Finally, we combine the ZANBA data and the Gigante et al. data to build a ML isoscape based on all the $^{87}Sr/^{86}Sr$ plant ratios currently available.

2. Previous research

2.1. Isoscape production

Isotopic analysis for the purpose of identifying the provenance and/or mobility patterns of biological specimens has been part of many disciplines' toolkits since the 1980s (Chisholm et al., 1986; Ericson, 1985; Graustein and Armstrong, 1983; Sealy et al., 1986). As more research was undertaken, the requirement of being able to relate the results of isotopic analysis to specific geographical locations or areas became increasingly apparent (Grupe et al., 1997; Price et al., 1994). In the 2000s, the use of isoscapes emerged (Bowen and Wilkinson, 2002; Bowen and Revenaugh, 2003; Dutton et al., 2005; Lykoudis and Argiriou, 2007; van der Veer et al., 2009), referring to maps of isotopic variation across regions that are produced by iteratively applying predictive models that estimate the local isotopic composition of environmental materials using empirical values from known coordinates (Bowen, 2010). Isoscapes were rapidly utilized to assess provenance and mobility of biological specimens (Fenner and Frost, 2009; Graham et al., 2010; Hobson et al., 2010; Rogers et al., 2012; Trueman et al., 2012). Major debates about issues such as the nature of immigration in the past continue to arise in the application of isoscapes (Madgwick et al., 2019; Barclay and Brophy, 2020; Madgwick et al., 2021; Evans et al., 2022), highlighting the need for isoscapes to be both accurate and interpreted correctly.

2.2. Machine learning in isoscape production

Compared to traditional geostatistical tools, such as Kriging interpolation, ML models exploit labelled datasets, including environmental and geological information, to predict the isotopic ratios of areas with similar features over a predetermined spatial range. Specifically, pioneering works on the application of ML to predict isotopic distribution showed that Random Forest (RF) regression provides the lowest prediction errors (Bataille et al., 2018). RF is a tree-based supervised ML algorithm that builds numerous random decision trees with bootstrapped subsets of the original variables and observations. In addition to their superior performance, RF models offer another benefit, namely the capability to extract information directly from the dataset, specifically identifying which variable best predicts the Sr isotope ratio. This feature enables RF models to offer insights into the local Sr cycle, aiding in the identification of primary sources of bioavailable Sr. So far, RF has been used to model Sr isotope data from several regions worldwide (Barbarena et al., 2021; Funck et al., 2021; Käßner et al., 2023; Wang et al., 2023; Bataille et al., 2020; Gigante et al., 2023; Bataille et al., 2018; Armaroli et al., 2024).

2.3. Strontium isoscapes of Sardinia

Four recent strontium isoscapes have included or addressed Sardinia (Bataille et al., 2020; Gigante et al., 2023; Emery et al., 2018; Lugli et al., 2022), though only one has Sardinia as a research focus (Gigante et al., 2023). Emery et al. offer the first $^{87}Sr/^{86}Sr$ isoscape specifically for Italy, including Sicily and Sardinia (Emery et al., 2018). Their isoscape uses inverse distance weighting to interpolate between 199 sampled Sr

isotope ratios and covers a total land area of 294,140 km^2 (Central Intelligence Agency, 2023), averaging one known Sr isotope ratio per 1478 km^2. The values come from published studies of diverse strontium archives, including sediments, spring waters, archaeological human and faunal remains, and modern foodstuffs. The authors acknowledge the problems inherent in combining values for bioavailable and non-bioavailable Sr and offer their map as a preliminary first step in provenance and mobility studies in Italy.

While Emery et al.'s sampled Sr isotope ratios are geographically well distributed for much of peninsular Italy, the isoscape for Sardinia is based on a small number of tightly clustered values, placing almost the entirety of Sardinia within a single $^{87}Sr/^{86}Sr$ range (0.7123–0.7157). These results are not problematic for Emery et al.'s research goals, which do not include Sardinia, but they do mean that Emery et al.'s isoscape does not provide sufficient resolution for even preliminary provenance and mobility studies on Sardinia. The Emery et al. isoscape is therefore not evaluated in this study.

Bataille et al.'s global Sr isoscape (Bataille et al., 2020) offers another possibility for interpreting empirical results from Sardinian samples. Their isoscape is offered as an advance toward more accurate isoscape development rather than as a finished product for any specific area: the authors explicitly recommend their isoscape for broad scale approaches, particularly for informing where additional targeted sampling for specific research questions should be undertaken, and they note that the extrapolation may not be valid in geologically complex and data-poor regions, both of which would characterize Sardinia at the time they produced the isoscape. Only five empirical values from Sardinia were incorporated into the production of the global isoscape, all of which were taken on rock. We therefore acknowledge that by evaluating the Bataille et al. isoscape against empirical plant data from Sardinia, we are not using directly comparable data. However, the global map was intended for broader use than predicting lithological values, and the fact that an isoscape is now available for the entire globe has prompted its relatively widespread use for interpretation, sometimes without additional training or validation. It is therefore useful to consider the results of such an application in a geologically diverse area such as Sardinia.

Lugli et al. (Lugli et al., 2022) offer an isoscape of Italy that is an expansion of Emery et al.'s database, using both novel and previously published data to arrive at 1920 sampled values from 777 locations, an average of one empirical value per 387 km^2. The sampled values include both bioavailable and nonbioavailable sources of Sr. To interpolate their isoscape, Lugli et al. employ Ordinary Kriging and Universal Kriging, this latter drifted by a geolithological map built ad-hoc. They acknowledge that bioavailable Sr data is preferable when building isoscapes to provenance biological tissues, and therefore produce two maps, one using exclusively bioavailable data and one that includes both bioavailable and nonbioavailable Sr ratios. Overall, they find that Universal Kriging with external drift produced the best map, with the lowest root mean squared errors (RMSE) being associated with the Universal Kriging map based on the bioavailable samples, although the difference was not substantial.

With respect to Sardinia specifically, Lugli et al.'s isoscape does not improve substantially on Emery et al.'s isoscape. Lugli et al. include one additional Sr isotope ratio from the northwest of the island, but otherwise they rely on the same five tightly clustered samples used by Emery et al. Lugli et al. acknowledge that the number of samples for Sardinia is insufficient, and they exclude Sardinia from their Ordinary Kriging interpolation. They also note that the largest model errors for their maps come from Sardinia and Sicily due to the low numbers of values for these areas. Their interpolated Sr isotope ratios for Sardinia range approximately 0.7115–0.7143 in the bioavailable map and approximately 0.7124–0.7147 in the map that includes the nonbioavailable values.

Gigante et al. (Gigante et al., 2023) offer the only previous Sardinia-specific isoscape in the literature. Their isoscape covers 5227 km^2 of southern Sardinia and is built using 30 novel Sr isotope ratios from modern plants using a ML approach with a Random Forest algorithm based on 6 external predictors selected from a possible 21 by the *VSURF* R package. The sampling density of the map is 1 sample per 174 km^2 with the samples clustered primarily around the east and south coasts of Sardinia's Sulcis region. The modelled values range between 0.70927 and 0.71190.

3. Materials and methods

3.1. Selection of the sampling area

The lithology of the island of Sardinia is complex. The *Carta Geologica di base della Sardegna in scala 1:25.000 (Carta Geologica)* (Carta Geologica di base della Sardegna in scala 1:25.000, 2008) identifies 777 unique bedrock categories that range in age from Quaternary deposits of gravels, sands, and silts to Precambrian-Palaeozoic mica-schists. The goal of the current study was to produce a densely sampled isoscape, making the sampling of the entirety of such a geologically varied island unfeasible. The sampling area was therefore defined as the section of Sardinia that falls between 39.5° and 40° N latitude, a total of approximately 6580 km^2 (Fig. 1). Over a third of the age categories of bedrocks on Sardinia identified by the *Carta Geologica* (Carta Geologica di base della Sardegna in scala 1:25.000, 2008) are present in the study area (Fig. 2). Because the age of the rock is the most important factor determining its $^{87}Sr/^{86}Sr$ ratio, the study area was judged to provide good regional coverage while also serving as a potential starting point for mapping the rest of the island.

The original data in this paper was produced by the Marie Skłodowska-Curie funded project ZANBA: ZooArchaeology of the Nuragic Bronze Age. The sampling area includes the primary archaeological site studied by ZANBA, Nuraghe Sa Conca 'e sa Cresia (Siddi (SU)) (Holt and Perra, 2021; Holt et al., 2022), as well as several sites where human and animal remains have been the subjects of previous carbon ($\delta^{13}C$), nitrogen ($\delta^{15}N$), and oxygen ($\delta^{18}O$) isotope studies (Atzeni et al., 2013; Lai et al., 2011; Lai et al., 2014; Lai et al., 2017).

3.2. Defining sampling domains and selecting sampling targets

The defined sampling area included 53 distinct categories of bedrock ages as defined by the *Carta Geologica* (Carta Geologica di base della Sardegna in scala 1:25.000, 2008). *The Carta Geologica* notes some uncertainty about the age ranges assigned to fourteen of these categories; these categories were therefore excluded as potential sampling targets. All 14 of the excluded categories have correlates that are not considered uncertain, making it possible to extrapolate probable strontium isotope ratios for them. There was substantial chronological overlap among the 39 remaining bedrock categories, allowing them to be combined into broader groupings.

Strontium isotope ratios in parent bedrocks are mainly determined by the original rubidium/strontium content of the bedrock and its age; however, some studies have indicated that lithology rather than age is a better predictive variable for $^{87}Sr/^{86}Sr$ ratios (Willmes et al., 2018). We therefore grouped our 39 remaining bedrock categories by both age and lithology. Because of both the scope of the study and the nature of the data in the *Carta Geologica* (Carta Geologica di base della Sardegna in scala 1:25.000, 2008), it was necessary to combine bedrock lithologies at different chronological scales, and generally the more recent bedrock groupings are more precise. Of the 22 categories that resulted from this grouping, four categories covered extremely small portions of the study area and were therefore not targeted for sampling: Upper Eocene-Oligocene sedimentary; Mesozoic sedimentary; Late Palaeozoic-early Mesozoic conglomerates and sedimentary; and Late Palaeozoic limestones, metalimestones, and dolomites.

To characterize the strontium isotope ratios of each of the 18 remaining bedrock categories (Table 1), we selected target sampling points throughout the bedrock category. These target points were chosen arbitrarily to provide representative spatial distribution across the category while avoiding settlements and other areas where recent

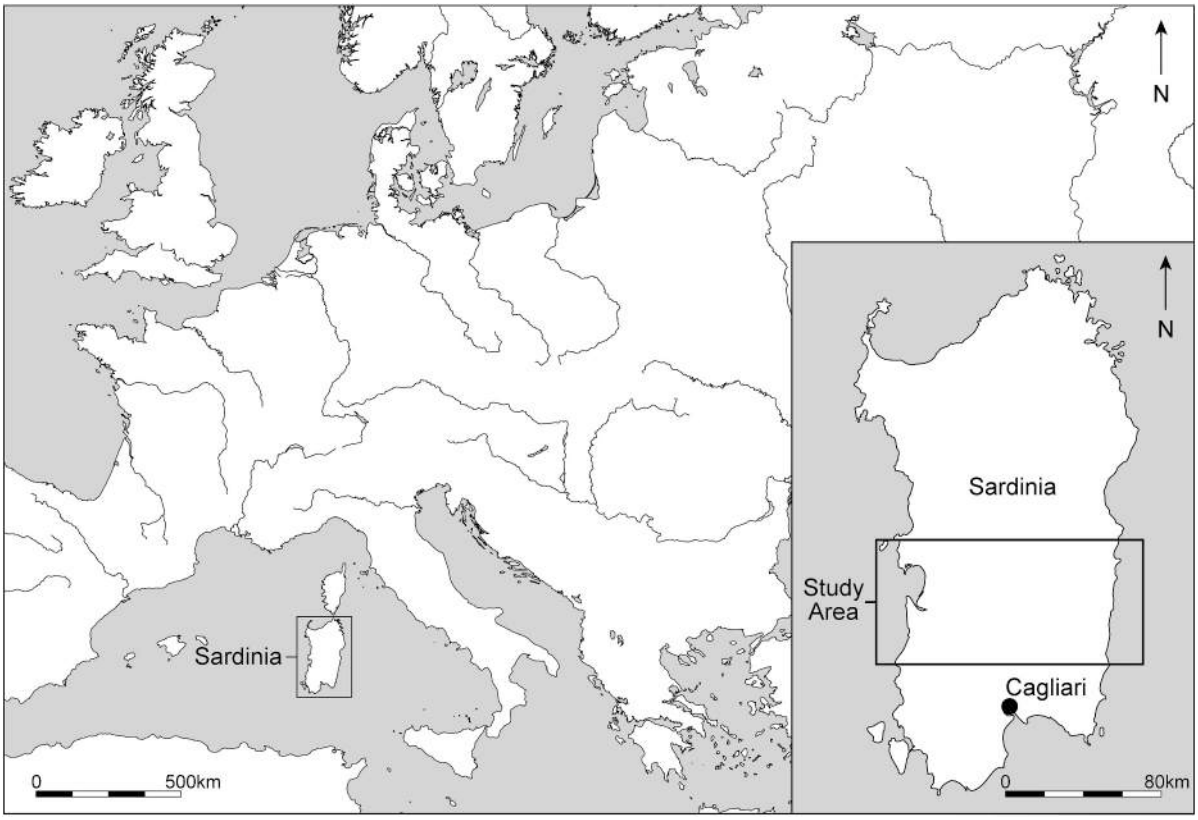

Fig. 1. The location and extent of the study area within the island of Sardinia.

human activities may have affected the composition of the sediments. A total of 128 target points were selected, approximately 1 sample per 52 km^2, making central Sardinia one of the most densely sampled areas for the creation of an isoscape globally (Fig. 2).

3.3. Archive selection and field collection

We chose modern plants as the archive to be sampled in preference to other commonly used archives such as surface waters, soil leachates, and sediments. A general consensus is emerging that, in much of the world, plants provide the best sources of bioavailable strontium for modeling isotopic values used to provenance terrestrial biological specimens (Britton et al., 2020; Evans et al., 2009; Maurer et al., 2012; Ryan et al., 2018). To minimize the potential effects of outliers, we followed a homogenized plant sampling methodology (Johnson, 2018). The sampling process took each target point as the center of a sampling area, which was defined as a 500 m radius around the target point. Within each sampling area, we selected three sub-sampling locations based, first, on a map-based assessment of the presence of vegetation, followed by a field assessment of the accessibility of areas with vegetation and the type of vegetation contained in the accessible areas. Sub-sampling locations were chosen to be as spread out as possible within the sampling area while taking into consideration the constraints of time and effort relative to their accessibility. Whenever possible, samples were taken as far as possible from roads and paths (Ryan et al., 2018). In addition, areas <50 m from rivers, streams or cultivated areas were avoided whenever possible (Britton et al., 2020; Sillen et al., 1998). Private properties, military areas, and protected ecological zones created further constraints in the choice of target points and sub-sampling locations. Use of GPS positioning and maps of lithological areas uploaded to a smartphone device ensured that samples were taken within the targeted lithological zones.

We preferred trees and shrubs that were 2–3 m tall for sampling because their root depths are more likely to avoid contaminating surface treatments (Britton et al., 2020; Johnson, 2018; Hartman and Richards, 2014), although not all studies have found significant differences between more deep- and more shallow-rooted plants (Willmes et al., 2018). Whenever possible, we sampled different tree and shrub species within a sampling area to avoid exaggerating any potential metabolic peculiarities of specific species. For each specimen, an average of ten leaves or small branches were collected and stored in a paper envelope. Details regarding sample species and sampling area were recorded in-field. In particular, we noted when ideal sampling standards could not be met (e.g. the sampling area was entirely cultivated, there was an absence of 2–3 m vegetation in the sampling area, the samples were taken <50 m away from rivers/roads).

3.4. Sample processing

We prepared samples for strontium isotope chemistry in the laboratories of Cardiff University BioArchaeology. First, the plants were freeze dried. Then, approximately 0.25–0.35 g of each plant was crushed by hand while wearing clean nitrile gloves and combined with samples of plants from the same sampling area, resulting in a mixed sample of approximately 1.0 g. For plant digestion and subsequent strontium analysis, samples were transferred to the clean laboratory (class 100, laminar flow) of the Cardiff Earth Laboratory for Trace Element and Isotope Chemistry (CELTIC). About 0.5 g of each mixed plant sample was transferred to a clean beaker and 2 mL of concentrated HNO_3 was added to begin the digestion process. A lid was placed on each beaker and partially tightened, allowing for gas to escape, and the samples were left to digest under a fume hood for at least a week. Next, 2 mL of 30–32 % H_2O_2 was added to each sample to continue the digestion process. A lid was placed on each sample and partially tightened to allow gas to escape, and the samples were left to digest under a fume hood for at least 2–3 days. Finally, the lids were removed, and the samples were placed

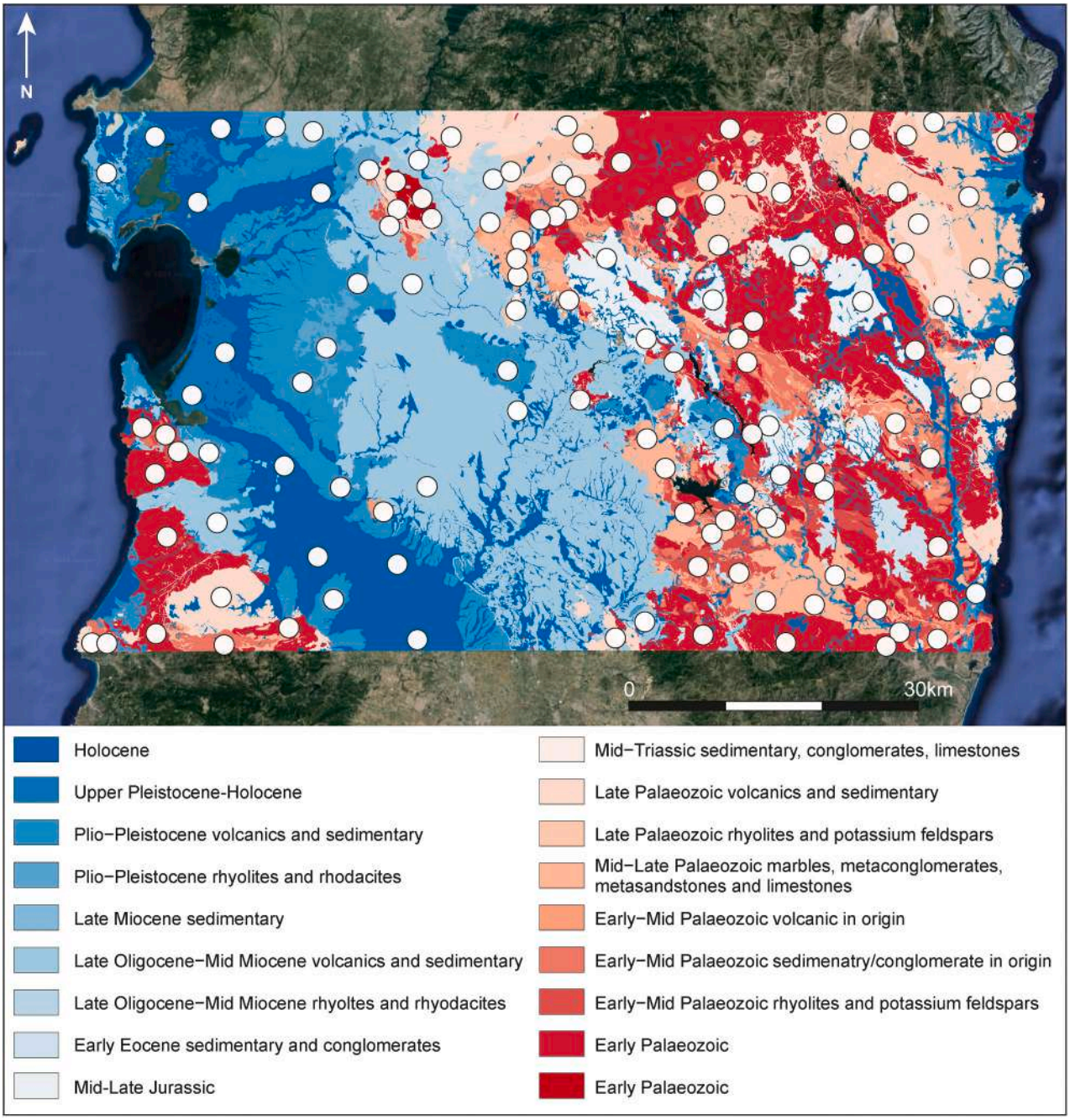

Fig. 2. The locations of the ZANBA sampling targets within the 18 bedrock categories.

on a hot plate to dry down, well spaced-out from each other to avoid possible contamination from bubbling as the samples dried.

After at least one day, when the samples were fully dried, 1 mL of 8 M HNO_3 was added to each sample, and the samples were covered with fully tightened lids and allowed to flux on a hot plate for at least one day until fully dissolved. The redissolved digested samples often included relatively large amounts of viscous organic material that was found to clog the columns during strontium extraction; the samples were therefore transferred to clean microcentrifuge tubes using unique clean pipette tips and centrifuged for 2–3 min. Only the liquid portion of the sample was transferred to the columns for strontium extraction. The presence of viscous material in the digested samples may indicate that not all organics were fully digested and that the results for each sampling target do not represent a precise 1:1:1 contribution from the three component plants.

Strontium extraction from plant samples used Sr.Spec™ resin using a revised version of protocol of Font et al. (Font et al., 2007). Matrix elements (including Ca and traces of Rb) were eluted in several washes of 8 M HNO3 and the samples placed on a hotplate (120 °C) overnight. This process was then repeated for a second pass to remove all remaining Ca. Once purified samples were dry, they were redissolved in 2 % HNO_3. Strontium isotope ratios were measured using a Nu Instruments Multi-Collector Inductively Coupled Plasma mass spectrometer (MC-ICP-MS). All data was first corrected for on-peak blank intensities, then mass bias corrected using the exponential law and a normalization ratio of 8.375209 for $^{88}Sr/^{86}Sr$ (Nier, 1938). Residual krypton (Kr) and rubidium (^{87}Rb) interferences were monitored and corrected for using ^{82}Kr and ^{83}Kr ($^{83}Kr/^{84}Kr = 0.20175$ and $^{83}Kr/^{86}Kr = 0.66474$; without normalization) and ^{85}Rb ($^{85}Rb/^{87}Rb = 2.5926$), respectively. Analysis of NIST SRM 987 during the analytical session gave a $^{87}Sr/^{86}Sr$ value of

Table 1
The results of the ZANBA $^{87}Sr/^{86}Sr$ sampling strategy by bedrock category.

ZANBA Bedrock category	Number of samples in category	Median $^{87}Sr/^{86}Sr$ ratio	Mean $^{87}Sr/^{86}Sr$ ratio	Lowest $^{87}Sr/^{86}Sr$ ratio	Highest $^{87}Sr/^{86}Sr$ ratio	Description	Bedrock codes in the *Carta Geologica di base della Sardegna in scala 1:25.000*
Holocene	9	0.710333	0.710032	0.707065	0.712775	Holocene sediments linked to gravity, floods, winds, lakes, and beaches. Holocene travertines	a, a1, a1a, b, b2, ba, bb, bc, bn, bna, bnb, bnc, d, e, e2, e3, e5, ea, eb, g2, f1
Upper Pleistocene-Holocene	4	0.709505	0.709682	0.709143	0.710575	Upper Pleistocene-Holocene ancient beach deposits: Sands, sandstones, calcirudites, gravels with bivalves, gastropods, with subordinate sandy-silty deposits and coastal tin chalcilutites	g
Plio-Pleistocene volcanic and sedimentary	8	0.708069	0.708138	0.706657	0.710434	Plio-Pleistocene volcanics including basalts, porphyritic andesites, and scoriaceous breccias proximal to the eruptive centers. Plio-Pleistocene conglomerates, breccias, and sedimentary	BGFb, BGFc, BGR, BGRa, GPAa, RIU, RSR, UCU, ULA, ZEP, NBB, NCA, ORS2a, ORS2c, ORS2d, PVM1, PVM2a, PVM2b, PVM2c
Plio-Pleistocene rhyolite and rhyodacite	2	0.708839	0.708839	0.708208	0.709470	Plio-Pleistocene rhyolites and rhyodacites: rhyolites and rhyodacites from afiric to porphyritic, dacites and rhyodacites from afiric to slightly porphyritic	GPA, MSU
Late Miocene	1	–	–	0.709172	0.709172	Late Miocene sedimentary: limestones, clayey and arenaceous silts, marly clays, arenaceous marls and silts	CLS, CTS, SMR, SMRa
Late Oligocene-Mid Miocene volcanic and sedimentary	9	0.709049	0.709154	0.707256	0.710517	Late Oligocene-Mid Miocene volcanics: andesites, porphyrics, basalts and basaltic andesites. Late Oligocene-Mid Miocene tuffs and breccias. Late Oligocene-Mid Miocene sedimentary: sandstones, marls, and conglomerates. Late Oligocene-Mid Miocene limestones	AAZ, AAZa, ATU, ATZ, BDU, BNS, BPL2, BSU, BSUa, BSUb, DIU, ECI, JOR, MIA, MIR, MMN, PAM, PDDa, PDDb, RCU, SMIa, TGR, TTZ, USSe, VTT, ZAR, ARX, MIAa, MIRa, RMLa, SMI, USS, USSa, GST, GSTa, GSTb, GSTc, NLL1, NLL1a, NLL2, NLL2a, RML, RMLb, RRTb, RUNa, TDI, TILa, RRTa, USSf, USSg, VLG
Late Oligocene-Mid Miocene rhyolite and rhyodacite	3	0.709260	0.709203	0.709070	0.709280	Late Oligocene-Mid Miocene rhyolites and rhyodacites	ALJ, DUL, GHE, IOI, IRU, NVT, RUN, UZZ
Early Eocene sedimentary and conglomerate	2	0.710544	0.710544	0.710059	0.711030	Early Eocene sedimentary and conglomerates: coarse sandstones and polygenic conglomerates, clays and marls, and limestones	FMCa, FMCb, FMCc
Mid-Late Jurassic	6	0.709115	0.709050	0.708539	0.709296	Mid-Late Jurassic: dolomites, arenaceous dolomites, dolomitic limestones, very mature quartz and quartzarenite conglomerates	DOR, GNS
Mid-Triassic sedimentary, conglomerate, and limestone	1	–	–	0.709168	0.709168	Mid-Triassic: sandstones, argillites, silts, marly levels with chalk and polygenic conglomerates, Laminated limestones, finely stratified limestones and dolomitic limestones	BUN, MUK
Late Palaeozoic volcanic and sedimentary	13	0.711065	0.711534	0.710135	0.716199	Late Palaeozoic volcanics: granites, granitoids, granodiorites, quartz, gabbros, amphibolic tonalites. Late Palaeozoic sedimentary and conglomerates	ABS1a, ABS1b, ABS2a, ABS2b, ABS3, ap, fb, fg, fi, fp, fq, fz, GIN, GTU1, GTU4, LNU1, LNU1a, LNU1b, LNU1c, LNU1d, LNU2b, LNU2c, mg, MTR, OTUa, OTUb, OTUd, OTUe, pb, pe, PFDb, RRL, TPU, TTL, URD, VGD1e, VGD2a, VLDc, VLDd, VLDe, LUD, LUDa, LUDb, LUDc
Late Palaeozoic rhyolite and potassium feldspar	14	0.711488	0.711611	0.709614	0.714438	Late Palaeozoic with potassium feldspars. Late Palaeozoic with rhyolites. Late Palaeozoic deposits with mixed rhyolite and andesite/dacitic components	GTU2, GTU3, LNU1e, LNU2a, LNU2d, MDV, OTUc, OTUf, OVOb, VGD1b, VGD1c, PEU, PFDa, pr, pa, pp
Mid-Late Palaeozoic marble, metaconglomerate, and limestone	10	0.710611	0.710538	0.708006	0.711541	Mid-Late Palaeozoic: marbles, dolomite marbles, metapelites, metasandstones, metaconglomerates, limestones	ASU, CSA, CSAa, CSAb, FLU, MUX, PMN, PMNa, PMNb, PMNc, SGA, SGAa, SGAb, VLL
Early-Mid Palaeozoic volcanic in origin	8	0.711064	0.711234	0.710032	0.713050	Early-Mid Palaeozoic mostly volcanic origin: metamorphic derivatives of alkaline basalts and volcanic metagrovacche, alkaline metabasites in	ACNc, md, MGM, MSV, MSVb, ORRa, ORRb

(*continued on next page*)

Table 1 (*continued*)

ZANBA Bedrock category	Number of samples in category	Median $^{87}Sr/^{86}Sr$ ratio	Mean $^{87}Sr/^{86}Sr$ ratio	Lowest $^{87}Sr/^{86}Sr$ ratio	Highest $^{87}Sr/^{86}Sr$ ratio	Description	Bedrock codes in the *Carta Geologica di base della Sardegna in scala 1:25.000*
						the strands position and alkaline metagabbros	
Early-Mid Palaeozoic sedimentary and conglomerate	10	0.711241	0.711388	0.709694	0.713312	Early-Mid Palaeozoic mostly sedimentary and conglomerate origin: metapelites, fossiliferous carbonate metasiltites, metalimestones	ACN, ACNa, MGMa, MRV, MRVa, MSVa, MUZ, MUZa, MUZb, ORR, ORRc, OSI, PSR
Early-Mid Palaeozoic rhyolite and potassium feldspar	8	0.711967	0.712226	0.710796	0.715056	Early-Mid Palaeozoic: rhyolites and potassium feldspars: rhiodacytic porphyry, metariolites, afanitic metariolites, porphyritic gray-dark metariolites and metariodacites, metatuffs and metaepiclastites with varying degrees of alteration	mr, MSVc, PGS, PRF, PRFa, vs
Early Palaeozoic	18	0.711745	0.711903	0.707065	0.714497	Early Palaeozoic: all bedrock types	GEN, SVI, SVIa, SVIb
Precambrian-Palaeozoic	3	0.712741	0.712816	0.712723	0.712984	Precambrian-Palaeozoic: all bedrock types	df, mi, pn, sc
Not included in study	–	–	–	–	–	Holocene sediments related to recent anthropogenic activity with a high likelihood of chemical alterations not representative of the past. Lakes and unclassifiable areas. Bedrock types minimally represented within the study area.	H, h1i, h1m, h1n, h1r, h1u, ha, L, nc, BGFa, BRD, TUL, LCP, CIX

0.710292 ± 0.000007 (2σ, $n = 11$) and all data is corrected to a NIST SRM 987 values of 0.710248 (Avanzinelli et al., 2005). Total procedural blanks are typically <20 pg of Sr, which is negligible relative to the Sr in each sample. Accuracy of the method was assessed by measurement of $^{87}Sr/^{86}Sr$ in NIST SRM 1400 (Bone Ash), which gave a $^{87}Sr/^{86}Sr$ value of 0.713129 ± 0.000019 (2SD), which is consistent with all published values (0.713126 ± 0.000017, (Romaniello et al., 2015; Weber et al., 2018)). Additionally, EC-5, an in-house coral standard, has been run alongside the NIST SRM 1400, giving a $^{87}Sr/^{86}Sr$ value of 0.709162 ± 0.000020 (2SD, $n = 217$). Individual errors for the reported samples are similar to the 2 standard deviation of the NIST 1400 and EC-5.

3.5. Machine learning isoscapes

To build our $^{87}Sr/^{86}Sr$ isoscapes of Sardinia we used a Random Forest regression (RF) with multiple predictors (*randomForest* package) (Liaw and Wiener, 2002), following the method of Bataille et al. (2020) (Bataille et al., 2020). We developed two distinct models: one using solely the empirical data from ZANBA, and another incorporating the empirical data from Gigante et al. (Gigante et al., 2023). We did not incorporate the empirical data from Bataille et al. (Bataille et al., 2020) because this data came from non-plant archives (Fig. 3).

Ten and eight external variables respectively, obtained from global raster maps, were selected by *VSURF* based on their importance in predicting the $^{87}Sr/^{86}Sr$ ratio for the ZANBA-only and the combined datasets respectively. These variables were: *r.bouger* is the bouger anomaly; *r.cec* is the soil cation exchange capacity; *r.clay* is the clay soil content (weight %); *r.dust* is a multi-models average ($g.m^{-2}.yr^{-1}$) of atmospheric mineral aerosol; *r.minage_geol* and *r.maxage_geol* are the log of the minimum and maximum geological ages from GLiM (high-resolution Global Lithological Map) (Hartmann and Moosdorf, 2012); *r.pet* is the potential evapotranspiration; *r.srsrq1* is the predicted first quartile of the global $^{87}Sr/^{86}Sr$ model reported in (Bataille et al., 2014); *r.ssa* and *r.ssaw* are multi-models average of sea salt depositions (for more information on the variables refer to (Bataille et al., 2020)). The significance of predictors in the RF model is determined through two criteria: the *%IncMSE*, representing the proportional rise in cross-validation mean squared error when the values of a particular variable are randomly permuted, and the *IncNodePurity*, indicating the influence of a specific variable on tree-split purity. Model trees were generated with $n = 3$ variables at a time (*mtry* = 3). A 10-fold cross validation was then

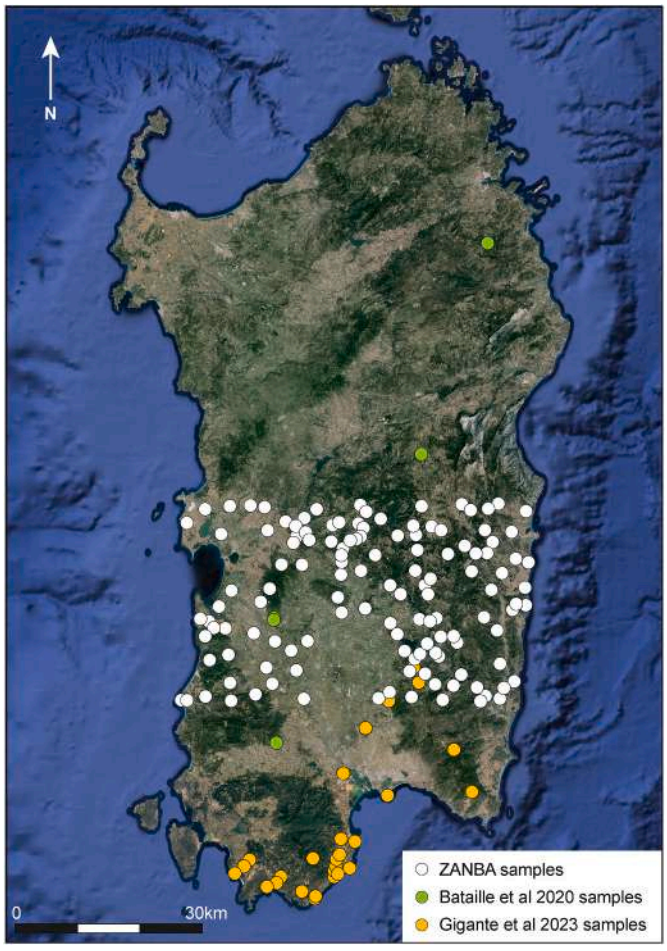

Fig. 3. The locations of the empirical data from ZANBA (plant archives), Gigante et al., 2023 (plant archives), and Bataille et al., 2020 (non-plant archives).

performed to check the prediction power of the models as RMSE (Root Mean Square Error). The RMSE of the ZANBA-only model and the ZANBA/Gigante et al. combined model were both equal to ~0.0012, with $R^2 = 0.5$. The associated spatial uncertainty maps were generated through a quantile RF regression (*ranger*) (Wright and Ziegler, 2017), calculated as half of the $q_{0.84}$ - $q_{0.16}$ difference (i.e. lower and upper limits of a ~ 68 % interval).

4. Results

4.1. ZANBA empirical data

The results of the ZANBA sampling are presented here by bedrock category using median and interquartile range, following the methodology of Evans et al. (Evans et al., 2023) Additionally, the mean ratios, lowest and highest ratios, and number of samples for each bedrock category are given in Table 1. Results for each of the individual target points are available as a spreadsheet in the supplementary materials.

The plant samples from 16 of the 18 bedrock categories gave median $^{87}Sr/^{86}Sr$ ratios ranging from 0.708069 (Plio-Pleistocene volcanic and sedimentary) to 0.712741 (Precambrian-Palaeozoic; Table 1). Two of the bedrock categories, Late Miocene bedrocks and Mid-Triassic sedimentary, conglomerate, and limestone bedrocks, were present in the study area in very small areas and were represented by a single plant sample each; a median ratio could therefore not be calculated for these categories. The sample for the Late Miocene bedrocks gave a $^{87}Sr/^{86}Sr$ ratio of 0.709172, and the sample for the Mid-Triassic sedimentary, conglomerate, and limestone bedrocks gave a $^{87}Sr/^{86}Sr$ ratio of 0.709168. Notably, the plants growing on the Upper Pleistocene-Holocene bedrocks (0.709505) and the plants growing on the Holocene sediments (0.710513) gave higher median values than might have been expected.

Interquartile ranges ranged from 0.0001 (Late Oligocene-Mid Miocene rhyolite and rhyodacite) to 0.0017 (Holocene). Broadly, plants growing on younger bedrocks and bedrocks with less parent Rb had smaller interquartile ranges and plants growing on older bedrocks and bedrocks with more parent Rb had larger interquartile ranges. Because the number of samples taken for each bedrock category differed widely, the Pearson correlation coefficient was used to assess whether the breadth of the interquartile range was correlated with the number of samples taken. The coefficient was calculated for the dataset both including ($n = 16$, $r = 0.529$ t-score $= 2.330$, p-value $= 0.035$) and excluding ($n = 11$, $r = 0.121$, t-score $= 0.366$, p-value $= 0.723$) bedrock categories with four or fewer samples, but in neither case was the correlation found to be significant. While the broad pattern holds, it is only very general, and it is noteworthy that the plants growing on the Holocene sediments had the largest interquartile range.

Overall, the plant ratios for the bedrock categories fall into two overlapping ranges (Fig. 4). The first range, ratios from 0.707143 to 0.710334, includes the Plio-Pleistocene volcanic and sedimentary bedrocks, the Plio-Pleistocene rhyolites and rhyodacites, the Late Oligocene-Mid-Miocene volcanic and sedimentary bedrocks, the Mid-Late Jurassic bedrocks, the Mid-Triassic sedimentary and conglomerate bedrocks and limestones, the Late Miocene bedrocks, the Late Oligocene-Mid-Miocene rhyolites and rhyodacites, and the Upper Pleistocene-Holocene bedrocks in order of lowest to highest median or single value where only one plant sample was analyzed. The second range, 0.710394 to 712,984, includes the Mid-Late Palaeozoic marbles, metaconglomerates, and limestones, the Early-Mid Palaeozoic volcanic in origin, the Late Palaeozoic volcanic and sedimentary bedrocks, the Early-Mid Palaeozoic sedimentary and conglomerate in origin, the Late Palaeozoic rhyolites and potassium feldspars, the Early Palaeozoic

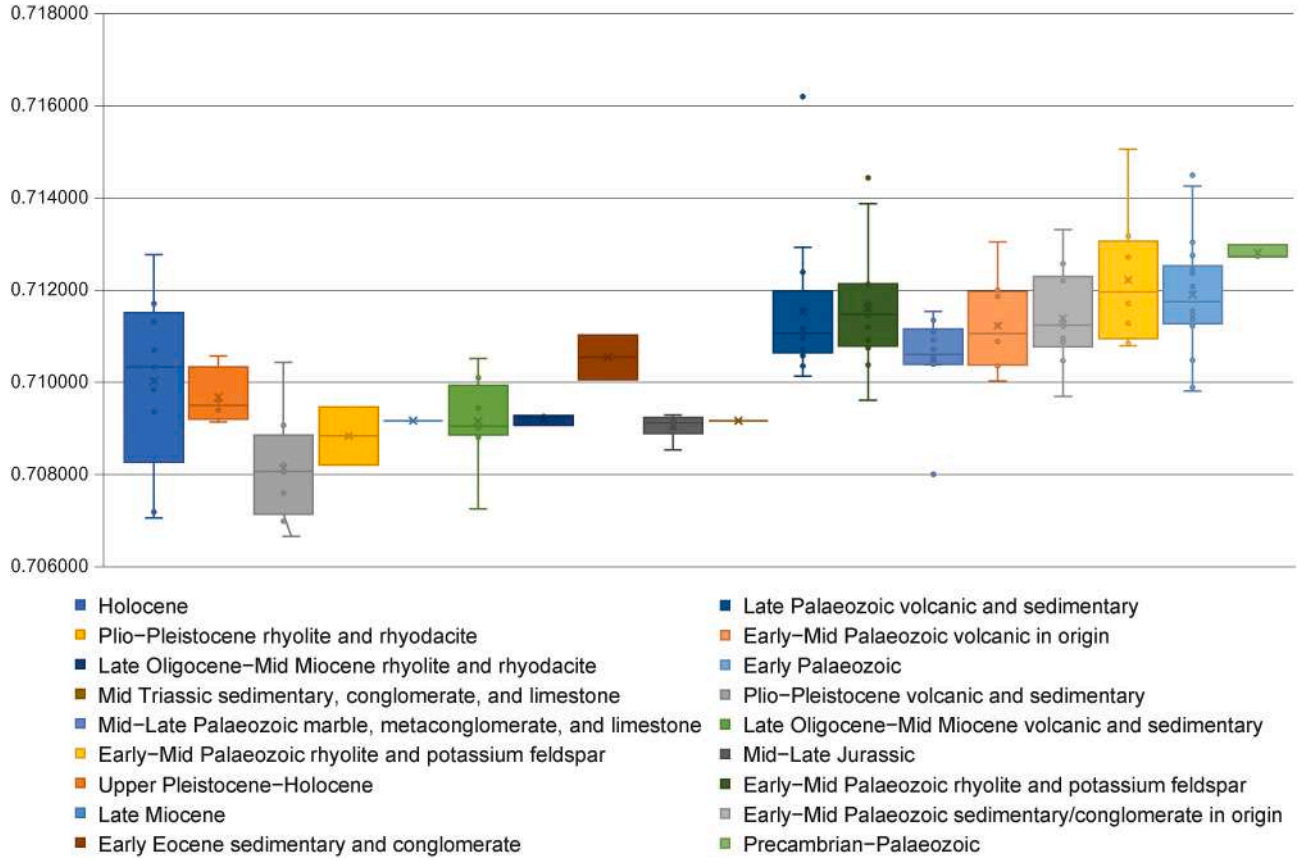

Fig. 4. The results of the ZANBA analyses by bedrock category showing the median, interquartile range, and outliers, following the methodology of Evans et al., 2023.

bedrocks, the Early-Mid Palaeozoic rhyolites and potassium feldspars, and the Precambrian-Palaeozoic bedrocks in order of lowest to highest median. The plant ratios for the Holocene sediments span much of both ranges, while the plant ratios for the Early Eocene sedimentary and conglomerate bedrocks span small parts of both ranges.

4.2. Machine learning isoscapes

We generated two new ML isoscapes (Fig. 5): the first built from the ZANBA data alone and the second built from the ZANBA data combined with the published $^{87}Sr/^{86}Sr$ ratios from Gigante et al. (Gigante et al., 2023). Because the entire island and not only the original ZANBA study area was modelled using the ZANBA data, the ZANBA-only isoscape has a sampling density of approximately 1 sample per 188 km^2. The isoscape modelled from the combined data has a sampling density of approximately 1 sample per 152 km^2. Both maps and their associated errors are available as GeoTIFFs 2–5 in the supplementary data.

The modelled ratios in the ML isoscape built from the ZANBA data alone range from 0.70746 to 0.71365, slightly contracting the empirical data, which includes five ratios <0.70746 and six ratios >0.71365. The modelled ratios in the ML isoscape built from the combined ZANBA and Gigante et al. (Gigante et al., 2023) data are similar, ranging from 0.70738 to 0.71375. In general, the inclusion of the Gigante et al. (Gigante et al., 2023) data tended to shift the predicted ratios lower in the fourth decimal place. Additionally, the inclusion of the data from Gigante et al. (Gigante et al., 2023) allowed the modeling of some parts of the island, particularly around the coasts, that were excluded when only the data from ZANBA were used.

5. Discussion

5.1. Holocene sediments in the ZANBA sampling area

One interesting characteristic of the ZANBA empirical results is the large interquartile range of the $^{87}Sr/^{86}Sr$ ratios of the plants growing on the Holocene sediments. There are several possible explanations for this. One explanation is that the parent bedrocks of these Holocene sediments may vary widely in age and composition, leading to a breadth of local $^{87}Sr/^{86}Sr$ ratios. Another possible explanation is that, as the primary locations of agriculture in central Sardinia, these sediments have been differentially affected by chemical treatments and fertilizers. The potential effects of agricultural treatments on the strontium composition of soils, surface waters, and groundwaters are well known (Zieliński et al., 2016; Böhlke and Horan, 2000; Blanz et al., 2019; Thomsen and Andreasen, 2019; Andreasen and Thomsen, 2021; Thomsen et al., 2021; Zieliński et al., 2021), and although we tried to avoid sampling in areas that were under cultivation or near cultivated fields, avoiding the influence of agriculture was difficult for Holocene sediments, which are the site of much of the larger-scale agriculture on Sardinia. However, the results from building the ML isoscapes would suggest that fertilizers are

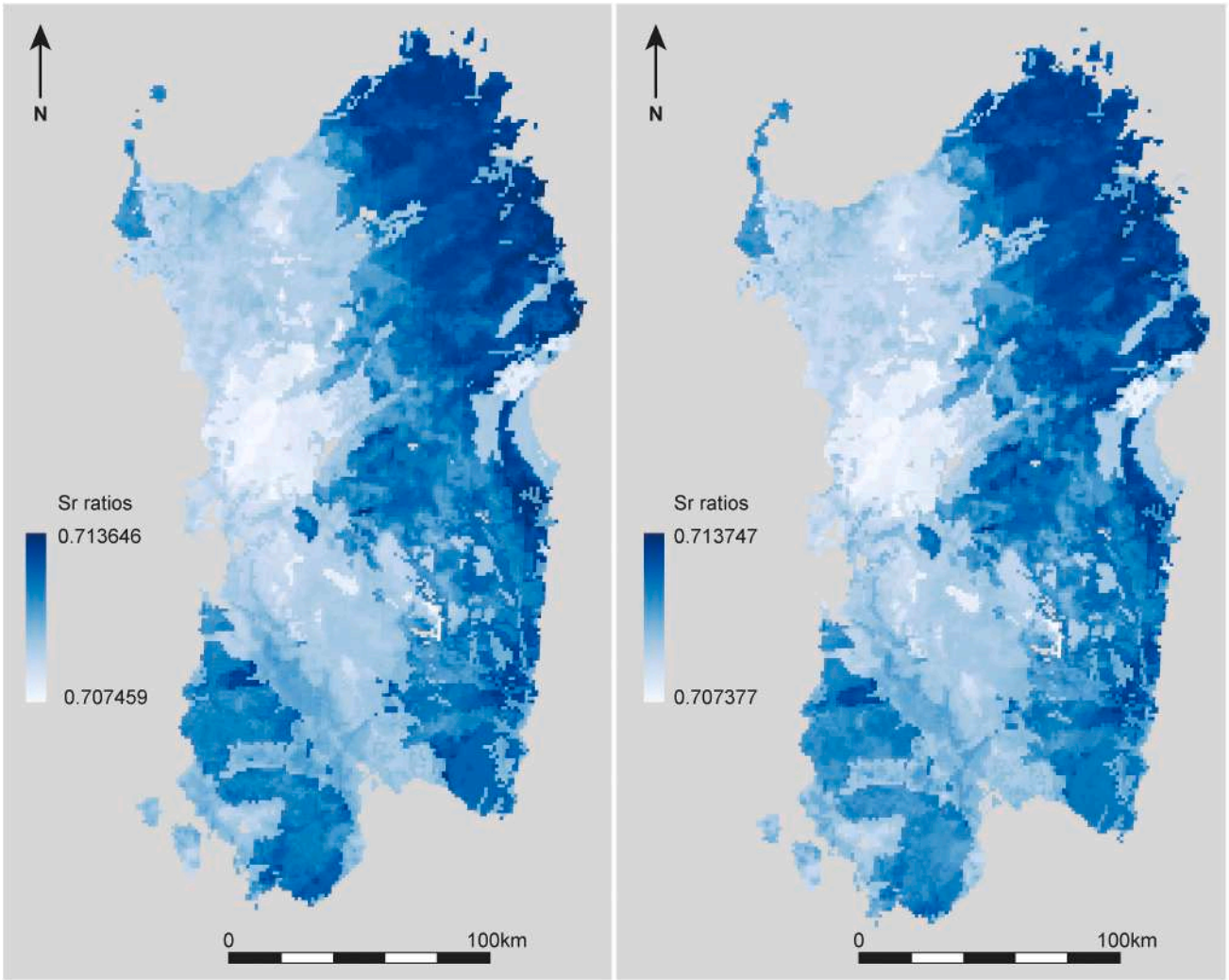

Fig. 5. The $^{87}Sr/^{86}Sr$ ratio ML isoscapes built from the ZANBA data (left) and from the combined data of ZANBA and Gigante et al., 2023 (right).

not the cause of the variation in the Holocene sediments. If fertilizers played a large role in affecting the $^{87}Sr/^{86}Sr$ ratios of the analyzed plants from any bedrock group, we would expect the *r.fert* and/or *r.pfert* variables to be selected by VSURF, which was not the case (see discussion below).

5.2. Machine learning isoscapes

The ten variables selected by VSURF for the ZANBA-only isoscape lead to interesting interpretations (Fig. 6). The selection of both *r.ssa* and *r.ssaw* suggests that sea spray is an important contributor to bioavailable strontium, as might be expected for an island. The same is true for *r.dust*, which may relate to seasonal summer winds carrying dust northward from the Sahara. The variable *r.pet* might also be expected given the hot summer temperatures and strong winds. However, the fact that the variable *r.fert*, which is the global nitrogen fertilization, was not selected suggests that the use of fertilizer did not affect the empirical data. We further tested this conclusion by adding the global phosphate fertilization *r.pfert* and rerunning the model (Potter et al., 2010; Potter et al., 2012); *r.pfert* was also not selected. Whether the failure of VSURF to

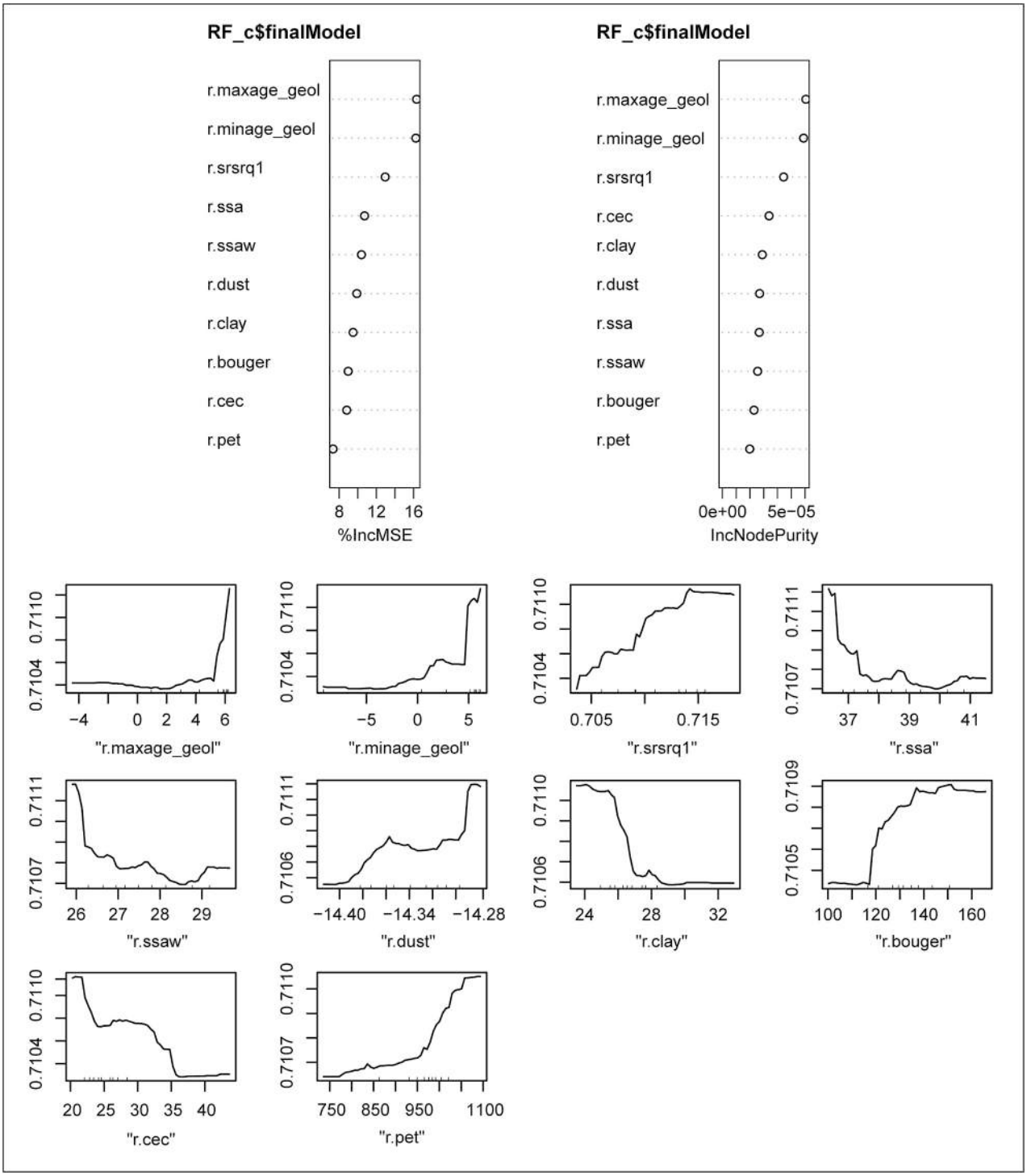

Fig. 6. Graphs of the importance of the variables and the partial dependences in the ZANBA-only ML isoscape produced by *VSURF*. These graphs represent the relationships between the Sr isotopes and each of the variables where it is at its maximum.

select either *r.fert* or *r.pfert* is because fertilizer is not an important component of bioavailable strontium in central Sardinia or whether it is because the ZANBA sampling strategy successfully avoided areas affected by fertilizer cannot be assessed with our data. Further research into the historical use of fertilizers in central Sardinia would be necessary to fully understand the *r.fert* and *r.pfert* results.

For the isoscape built from the combined ZANBA and Gigante et al. data, VSURF selects the same variables except that it does not identify *r.ssaw* and *r.pet* as affecting the model (Fig. 7). This may suggest that evapotranspiration has a more significant effect on bioavailable strontium in the interior of Sardinia that it does closer to the coasts.

5.3. Comparing isoscapes using empirical data

The dense sampling methodology employed by ZANBA gives us the opportunity to compare the modelled values from different densities of primary sampling, 1 point per 4818 km^2 (5 primary data points) in Bataille et al. (Bataille et al., 2020) and 1 point per 174 km^2 (30 primary data points) in Gigante et al. (Gigante et al., 2023), against the empirical $^{87}Sr/^{86}Sr$ ratios for specific locations in central Sardinia. Although the ZANBA sampling strategy was devised before Gigante et al. was published, 23 of ZANBA's sampling targets are made up of samples that fall completely within Gigante et al.'s (Gigante et al., 2023) modelled isoscape, and an additional three of ZANBA's sampling targets include one or two samples that fall within it. We therefore focused on these 26 points as a useful set to evaluate both the Bataille et al. (Bataille et al., 2020) and the Gigante et al. (Gigante et al., 2023) isoscapes.

To assess whether the modelled isoscapes correctly predicted the ZANBA empirical ratios, we established a range for each empirical ratio by adding and subtracting the empirical uncertainty from the empirical ratio. This empirical range was then compared to two sets of predicted ranges. The first set was the predicted value at the ZANBA target point +/− each isoscape's calculated uncertainty. The second set was intended to reflect the homogenized sampling strategy used by ZANBA, which meant that sometimes the three individual plant samples that were combined to make up the ratio representing the sampling target came from areas of the isoscapes with two or three different predictions and uncertainties/standard errors. Where this was the case, we calculated a

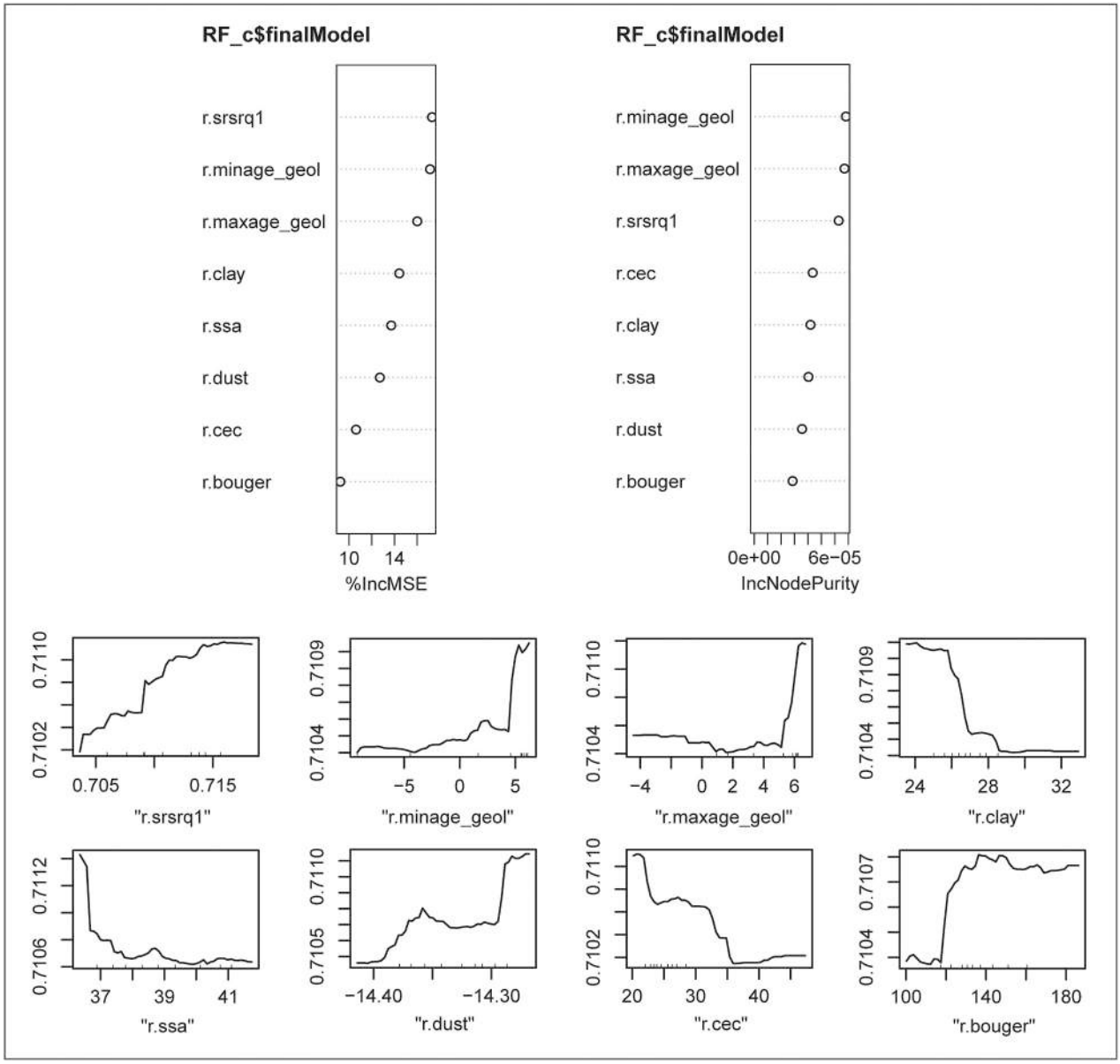

Fig. 7. Graphs of the importance of the variables and the partial dependences in the ZANBA/Gigante et al. combined ML isoscape produced by *VSURF*. These graphs represent the relationships between the Sr isotopes and each of the variables where it is at its maximum.

weighted arithmetic mean for the prediction, as well as a weighted arithmetic mean for the error. For example, if the three ZANBA samples that made up the ratio for Point X came from three different prediction and uncertainty zones, the prediction and uncertainty were $(X_1 + X_2 + X_3)/3$. However, if two of the samples came from one prediction zone and the third came from a different zone, the prediction and uncertainty were $((X_1*2) + X_2)/3$.

Comparing the ZANBA empirical ranges with the target point prediction ranges, Bataille et al. correctly predicted 10 of 26 ratios (average size of prediction range = 0.00243, Fig. 8a). One of the target points fell outside the Gigante et al. modelled isoscape, so using this method Gigante et al. correctly predicted 13 of 25 ratios (average size of prediction range = 0.00201, Fig. 8b). Comparing the ZANBA empirical ranges with the weighted average prediction ranges, Bataille et al. correctly predicted 9 of 26 ratios (average size of prediction range = 0.00243, Fig. 9a) and Gigante et al. correctly predicted 14 of 26 (average size of prediction range = 0.00201, Fig. 9b).

The 30 $^{87}Sr/^{86}Sr$ ratios taken on plants published by Gigante et al. provide a similar opportunity to interrogate the Bataille et al. isoscape and the new isoscape produced from the ZANBA data. Of these 30 ratios, 26 came from areas modelled by the Bataille et al. and ZANBA isoscapes. The Bataille et al. isoscape correctly predicted 5 of the 26 ratios (average size of prediction range = 0.00176, Fig. 10a), while the ZANBA isoscape correctly predicted 16 (average size of prediction range = 0.00255, Fig. 10b).

In addition to assessing whether the isoscapes correctly predicted the empirical data, it is useful to assess the degree of inaccuracy of the incorrect predictions. To do this, we calculated a "miss size" that was the arithmetic mean of the amounts by which all the lowest or highest values of the incorrect prediction ranges for a given set were off from the highest or lowest values (respectively) of the ranges of the empirical data. Comparing the Bataille et al. and Gigante et al. isoscapes against the ZANBA empirical data, using the target point prediction method, Bataille et al.'s 16 incorrect predictions had a mean miss size of 0.00110 (range: 0.00002–0.00309), while Gigante et al.'s 12 incorrect predictions had a mean miss size of 0.00096 (range: 0.00004–0.00245). Using the weighted average prediction method, the Bataille et al. isoscape's 17 incorrect predictions had a mean miss size of 0.00187 (range:

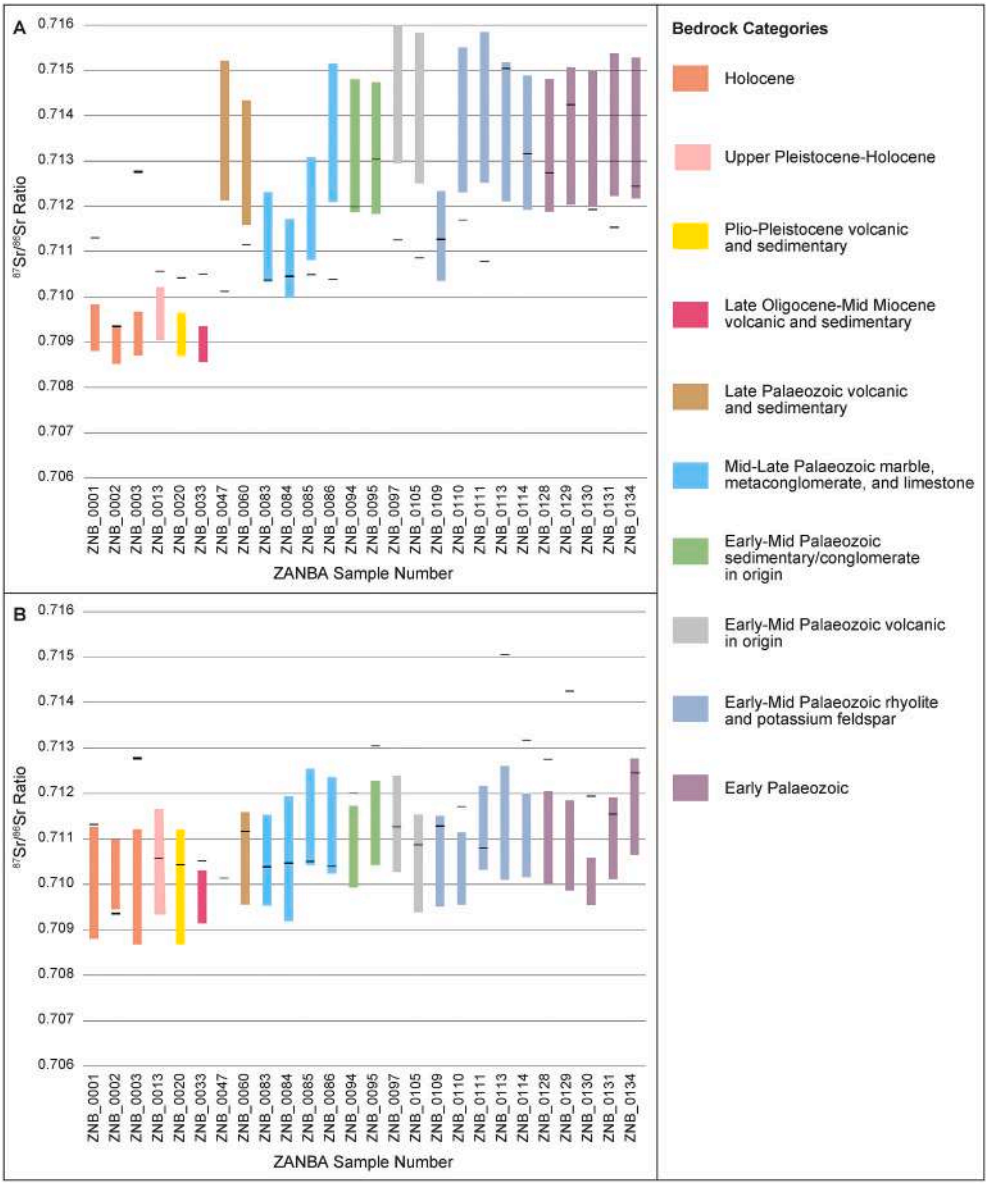

Fig. 8. ZANBA experimental $^{87}Sr/^{86}Sr$ ratio ranges (black lines) compared with A) Bataille et al., 2020 target point predicted ranges (colored bars, top panel) and B) Gigante et al., 2023 target point predicted ranges (colored bars, bottom panel).

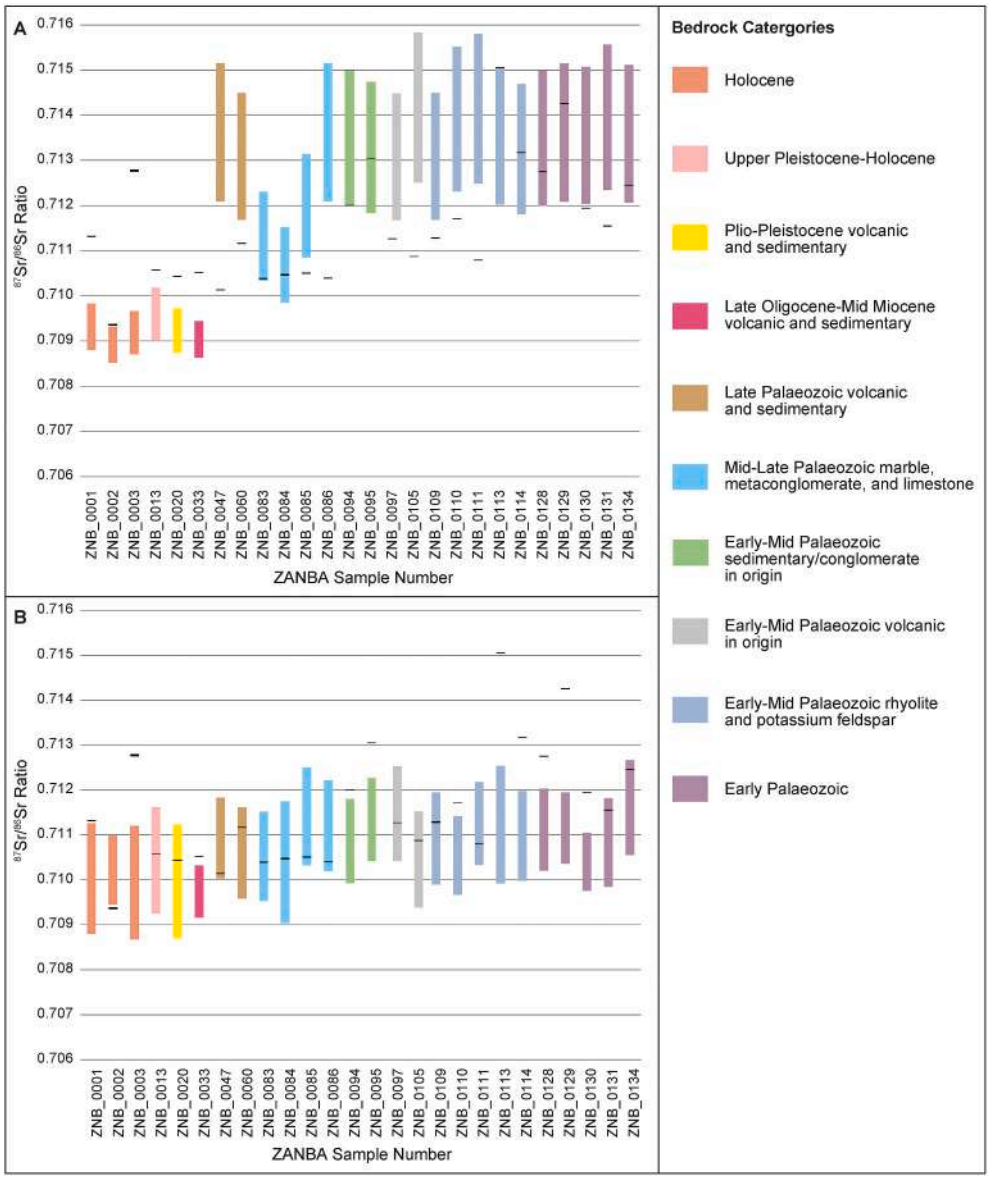

Fig. 9. ZANBA experimental $^{87}Sr/^{86}Sr$ ratio ranges (black lines) compared with A) Bataille et al., 2020 weighted average predicted ranges (colored bars, top panel) and B) Gigante et al., 2023 weighted average predicted ranges (colored bars, bottom panel).

0.00002–0.00309), while the Gigante et al. isoscape's 12 incorrect predictions had a mean miss size of 0.00089 (range: 0.00004–0.00250). These results are broadly comparable both between isoscapes and between prediction methods, though the Gigante et al. isoscape's incorrect predictions were slightly closer than those of the Bataille et al. isoscape. The Bataille et al. isoscape performed slightly better when evaluated with the target point prediction method, while the Gigante et al. isoscape performed slightly better when evaluated with the weighted average prediction method.

Considering the Bataille et al. and ZANBA isoscapes against the Gigante et al. empirical data, the Bataille et al. isoscape's 21 incorrect predictions had a mean miss size of 0.00112 (range: 0.00008–0.00257). The ZANBA isoscape's 10 incorrect predictions had a mean miss size of 0.00060 (range: 0.00009–0.00124).

It is important to note that the Bataille et al. isoscape was notably less accurate predicting the Gigante et al. empirical data than it was predicting the ZANBA empirical data, and that the average by which these predictions were off was similar. This is important because the average Root Mean Squared Error (RMSE) of the isoscape's predictions for the Gigante et al. empirical data was smaller than for the ZANBA empirical data (0.00088 vs. 0.00121 (TP)/0.00122 (WA)). In discussions of isoscapes, low RMSE's are often pointed to as indications that an isoscape is accurate (Bataille et al., 2018). The results of our study serve as a reminder that RMSE describes only the model and the data used to create it. If this data is unrepresentative in any way, the resulting isoscape may not be usable for interpretation despite low RMSE. With only 5 empirical values from Sardinia incorporated into the Bataille et al. isoscape, it is clear that – in this case – the data is unrepresentative, whatever the RMSE. However, in other isoscapes, the non-representativeness of the data may be less apparent. RMSE should therefore not be emphasized as expressing the real-world validity and applicability of an isoscape. Independent spatial validation with additional data is needed even for isoscapes with low RMSE before they can be used confidently for interpretation.

5.4. Using isoscapes to interpret new data

The improved accuracy of predictions demonstrated by comparing the isoscapes of Bataille et al. (5 empirical ratios from Sardinia), Gigante et al. (30 empirical ratios), and ZANBA (128 empirical ratios) strongly

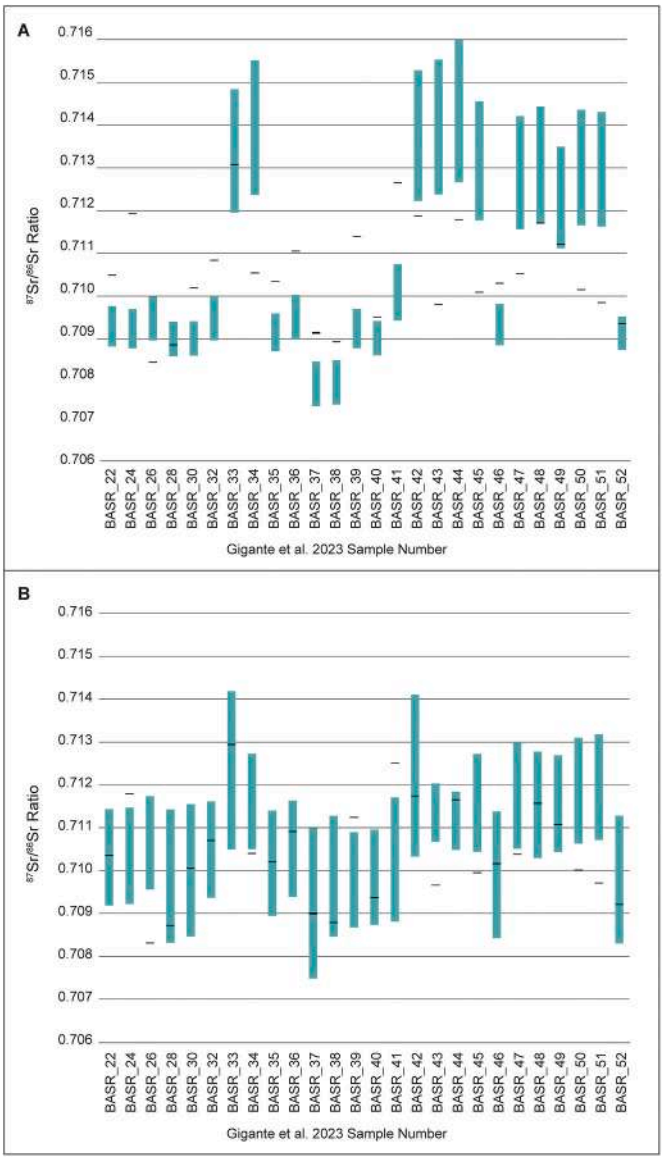

Fig. 10. Gigante et al., 2023 experimental $^{87}Sr/^{86}Sr$ ratio ranges (black lines) compared with A) Bataille et al., 2020 predicted ranges (teal bars, top panel) and B) ZANBA machine learning isoscape predicted ranges (teal bars, bottom panel).

suggests that increasingly accurate isoscapes can be produced from sufficient samples using the Random Forest ML method developed by Bataille et al. (Bataille et al., 2020). However, the improvement between the Gigante et al. isoscape (14 correct predictions, average prediction inaccuracy of 0.000892624) and the ZANBA isoscape (16 correct predictions, average prediction inaccuracy of 0.000598642) is not as great as might be expected given that the ZANBA isoscape is built from four times as many empirical ratios. In both cases, the isoscapes were built from empirical ratios taken at locations that were relatively far away from the locations of the empirical ratios used to test them. These findings suggest that sampling density must be balanced with sample distribution to achieve isoscapes accurate enough to use for interpretation. More specific recommendations relating the complexity of an area's geology with the density of samples required to produce accurate isoscapes will require additional research but represent a fruitful direction of future study.

Despite the demonstrable improvement in accuracy between the Gigante et al. and ZANBA isoscapes, the overall accuracy of these Sardinia-specific isoscapes remains problematic. Fourteen and 16 correct predictions out of a possible 26 is only a little better than could be expected from estimating based on lithological character. However, these results may give an overly pessimistic view of the accuracy of isoscapes in general. Sardinia has a complex geology compressed into a relatively small area: a possible reason why the densely sampled ZANBA landscape did not create a substantially more accurate isoscape than the moderately densely sampled landscape of Gigante et al. is that the ZANBA bedrock categories may have been over-grouped, and therefore the samples did not fully reflect the complexity of the geology despite their density. Isoscapes built from empirical values sampled from less complex geologies may be more accurate.

It is also important to consider that plant samples were used to assess the accuracy of the isoscapes. Plants are prone to outliers (Lahtinen et al., 2021), a problem that homogenized sampling was developed to address. It is possible that the ML maps in this study would have performed better in predicting the strontium ratios of local animals, whose feeding patterns would average the ratios of the plants, other foods, and waters consumed. Evaluating plant-based isoscapes against animal samples from individuals with known feeding patterns is an important next step in confirming the isoscapes' interpretive potential and the degree to which they are generalizable across specimen types.

Our results indicate the importance of multi-isotope studies to assess provenance at this stage of isotope research. Isoscapes of individual isotopic ratios are likely to be less accurate than we hope they are, with the resulting single-isotope studies prone to interpretive error. Many researchers already employ a probabilistic assessments of multi-isotope studies to assess provenance (Laffoon et al., 2017). Such methods will always be important in isotopic studies given the exclusionary nature of isotopic provenancing; however, we would argue that probabilistic assessments of multi-isotope studies are currently essential for interpretation and will remain so until individual isoscapes are demonstrated to have sufficient predictive accuracy. We would also argue that the validation and refinement of existing isoscapes represents a next phase of research leading toward successful provenancing.

6. Conclusions

The comparison of ML isoscapes presented here is encouraging while simultaneously serving as a cautionary tale. Increasing the number of empirical $^{87}Sr/^{86}Sr$ ratios did improve the accuracy of ML isoscapes; however, there was a clear problem of diminishing returns. Further methodological research is necessary to understand how the accuracy of ML isoscapes can be improved beyond simply including more samples. We also found that low RSME was not inherently an indication of an accurate isoscape and should not be used uncritically as such. To conclude, we emphasize, as have the authors of all the isoscapes discussed in this paper, that any isoscape we produce is a step toward an optimal isoscape rather than a final product. We hope that the isoscape of Sardinia built from the combined empirical data from ZANBA and Gigante et al., which is available in the supplementary materials, will serve as an inspiration for the collection of further empirical data and subsequent refinement of both general methodologies and specific isoscapes.

Supplementary data to this article can be found online at https://doi.org/10.1016/j.scitotenv.2025.179880.

CRediT authorship contribution statement

Emily Holt: Writing – review & editing, Writing – original draft, Visualization, Project administration, Methodology, Investigation, Funding acquisition, Formal analysis, Data curation, Conceptualization. **Federico Lugli:** Writing – review & editing, Writing – original draft, Visualization, Software, Methodology, Formal analysis. **Davide Schirru:** Writing – review & editing, Writing – original draft, Resources, Investigation. **Melania Gigante:** Writing – review & editing, Resources.

Katie Faillace: Writing – review & editing, Investigation. **Marc-Alban Millet:** Writing – review & editing, Writing – original draft, Resources, Investigation. **Morten Andersen:** Writing – review & editing, Resources, Investigation. **Richard Madgwick:** Writing – review & editing, Writing – original draft, Supervision, Project administration, Methodology, Funding acquisition, Data curation, Conceptualization.

Funding sources

This project has received funding from the European Union's Horizon 2020 research and innovation programme under grant agreement No 839517.

Declaration of competing interest

The authors declare that they have no known competing financial interests or personal relationships that could have appeared to influence the work reported in this paper.

Acknowledgements

We would like to gratefully acknowledge the support of the Soprintendenza Archeologia, belle arti e paesaggio per la città metropolitana di Cagliari e le province di Oristano e Sud Sardegna in conducting this research, particularly Francesca Candilio. We would also like to thank Jane Evans, for her advice while we were deciding how to group the bedrock categories used in our sampling strategy, and Kirsty Harding, for preparing the figures in the article. Holt would like to thank Judith Sealy, Petrus Le Roux, Kerryn Gray, Max Spies, and the participants of the workshop *Strontium Isoscapes for Mobility and Migration: The Way Forward (Cape Town, 29 January – 2 February 2024)*, which was influential in shaping this article. Finally, we would like to thank the three anonymous reviewers whose comments helped us improve this manuscript.

Data availability

The data is made available in the supplementary materials.

References

Andreasen, R., Thomsen, E., 2021. Strontium is released rapidly from agricultural lime–implications for provenance and migration studies. Front. Ecol. Evol. 8 (588422). https://doi.org/10.3389/fevo.2020.588422.

Armaroli, E., Lugli, F., Cipriani, A., Tütken, T., 2024. Spatial ecology of moose in Sweden: combined Sr-OC isotope analyses of bone and antler. PLoS One 19, e0300867. https://doi.org/10.1371/journal.pone.0300867.

Atzeni, E, Usai, A, Bellintani, P, Fonzo, O, Lai, L, Tykot, RH et al Le Tombe Nuragiche di Sa Sedda 'e Sa Caudela (Collinas - CA). Scavi 1982–84. Soprintendenza per i Beni Archeologici per le Province di Cagliari e Oristano Quaderni 23 2007–2012. Cagliari: Ministero per I Beni e le Attivita Culturali; 2013. pp. 28–54.

Avanzinelli, R., Conticelli, S., Francalanci, L., Boari, E., 2005. High precision Sr, Nd, and Pb isotopic analyses and reproducibility using new generation thermal ionisation mass spectrometer: aims and perspective for isotope geology applications. Period Mineral. 74, 147–166.

Barbarena, R., Cardillo, M., Lucero, G., LeRoux, P.J., Tessone, A., Llano, C., et al., 2021. Bioavailable strontium, human paleogeography, and migrations in the southern Andes: a machine learning and GIS approach. Front. Ecol. Evol. 9 (584325). https://doi.org/10.3389/fevo.2021.584325.

Barclay, G.J., Brophy, K., 2020. 'A veritable chauvinism of prehistory': nationalist prehistories and the 'British' late Neolithic mythos. Archaeol. J. 1–31. https://doi.org/10.1080/00665983.2020.1769399.

Bataille, C.P., Brennan, S.R., Hartmann, J., Moosdorf, N., Wooller, M.J., Bowen, G.J., 2014. A geostatistical framework for predicting variations in strontium concentrations and isotope ratios in Alaskan rivers. Chem. Geol. 389, 1–15. https://doi.org/10.1016/j.chemgeo.2014.08.030.

Bataille, C.P., von Holstein, I.C.C., Laffoon, J.E., Willmes, M., Xiao-Ming, L., Davies, G.R., 2018. A bioavailable strontium isoscape for Western Europe: a machine learning approach. PLoS One 13, e0197386. https://doi.org/10.1371/journal.pone.0197386.

Bataille, C.P., Crowley, B.E., Wooller, M.J., Bowen, G.J., 2020. Advances in global bioavailable strontium isoscapes. Palaeogeogr. Palaeoclimatol. Palaeoecol. 555, 109849. https://doi.org/10.1016/j.palaeo.2020.109849.

Blanz, M., Ascough, P., Mainland, I., Martin, P., Taggart, M.A., Dieterich, B., et al., 2019. Seaweed fertilization impacts the chemical and isotopic composition of barley: implications for analyses of archaeological skeletal remains. J. Archaeol. Sci. 104, 34–44. https://doi.org/10.1016/j.jas.2019.02.003.

Böhlke, J.K., Horan, M., 2000. Strontium isotope geochemistry of groundwaters and streams affected by agriculture, Locust Grove, MD. Appl. Geochem. 15, 599–609. https://doi.org/10.1016/S0883-2927(99)00075-X.

Bowen, G.J., 2010. Isoscapes: spatial pattern in isotopic biogeochemistry. Annu. Rev. Earth Planet. Sci. 38, 161–187. https://doi.org/10.1146/annurev-earth-040809-152429.

Bowen, G.J., Revenaugh, J., 2003. Interpolating the isotopic composition of modern meteoric precipitation. Water Resour. Res. 39, 1299. https://doi.org/10.1029/2003WR002086.

Bowen, G.J., Wilkinson, B., 2002. Spatial distribution of δ18O in meteoric precipitation. Geology 30, 315–318. https://doi.org/10.1130/0091-7613(2002)030<0315:SDOOIM>2.0.CO;2.

Britton, K., Le Corre, M., Willmes, M., Moffat, I., Grün, R., Mannino, M.A., et al., 2020. Sampling plants and malacofauna in 87Sr/86Sr bioavailability studies: implications for isoscape mapping and reconstructing of past mobility patterns. Front. Ecol. Evol. 8 (579473). https://doi.org/10.3389/fevo.2020.579473.

Carta Geologica di base della Sardegna in scala 1:25.000, 2008. Available. http://www.sardegnageoportale.it/index.php?xsl=2420&s=40&v=9&c=14479&es=6603&na=1&n=100&esp=1&tb=14401.

Central Intelligence Agency, 2023. Italy. In: The World Factbook [Internet] [cited 17 Dec 2023]. Available. https://www.cia.gov/the-world-factbook/countries/italy/#geography.

Chisholm, B., Driver, J., Dube, S., Schwarcz, H.P., 1986. Assessment of prehistoric Bison foraging and movement patterns via stable-carbon isotopic analysis. Plains Anthropol. 31, 193–205. https://doi.org/10.1080/2052546.1986.11909302.

Dutton, A., Wilkinson, B.H., Welker, J.M., Bowen, G.J., Lohmann, K.C., 2005. Spatial distribution and seasonal variation in 18O/16O of modern precipitation and river water across the conterminous United States. Hydrol. Process. 19, 4121–4146. https://doi.org/10.1002/hyp.5876.

Emery, M.V., Stark, R.J., Murchie, T.J., Elford, S., Schwarcz, H.P., Prowse, T.L., 2018. Mapping the origins of Imperial Roman workers (1st–4th century CE) at Vagnari, southern Italy, using 87Sr/86Sr and d18O variability. Am. J. Phys. Anthropol. 166, 837–850. https://doi.org/10.1002/ajpa.23473.

Ericson, J.E., 1985. Strontium isotope characterization in the study of prehistoric human ecology. J. Hum. Evol. 14, 503–514. https://doi.org/10.1016/S0047-2484(85)80029-4.

Evans, J.A., Montgomery, J., Wildman, G., 2009. Isotope domain mapping of $^{87}Sr/^{86}Sr$ biosphere variation on the Isle of Skye, Scotland. J. Geol. Soc. 166, 617–631. https://doi.org/10.1144/0016-76492008-043.

Evans, J.A., Pashley, V., Mee, K., Wagner, D., Parker Pearson, M., Fremondeau, D., et al., 2022. Applying lead (Pb) isotopes to explore mobility in humans and animals. PLoS One 17, e0274831. https://doi.org/10.1371/journal.pone.0274831.

Evans, J.A., Mee, K., Chenery, C.A., Marchant, A.P., 2023. User guide for the biosphere isotope domains GB dataset and web portal. British Geological Survey 35 (Report No.: OR/22/036).

Fenner, J.N., Frost, C.D., 2009. Modern Wyoming plant and pronghorn isoscapes and their implications for archaeology. J. Geochem. Explor. 102, 149–156. https://doi.org/10.1016/j.gexplo.2008.09.003.

Font, L., Nowell, G.M., Pearson, D.G., Ottley, C.J., Willis, S.G., 2007. Sr isotope analysis of bird feathers by TIMS: a tool to trace bird migration paths and breeding sites. J. Anal. At. Spectrom. 22, 513–522. https://doi.org/10.1039/B616328A.

Funck, J., Bataille, C.P., Rasic, J., Wooller, M., 2021. A bio-available strontium isoscape for eastern Beringia: a tool for tracking landscape use of Pleistocene megafauna. J. Quat. Sci. 36, 76–90. https://doi.org/10.1002/jqs.3262.

Gigante, M., Mazzariol, A., Bonetto, J., Armaroli, E., Cipriani, A., Lugli, F., 2023. Machine learning-based Sr isoscape of southern Sardinia: a tool for bio-geographic studies at the Phoenician-Punic site of Nora. PLoS One 18, e0287787. https://doi.org/10.1371/journal.pone.0287787.

Graham, B.S., Koch, P.L., Newsome, S.D., McMahon, K.W., Aurioles, D., 2010. Using isoscapes to trace the movements and foraging behavior of top predators in oceanic ecosystems. In: West, J., Bowen, G., Dawson, T., Tu, K. (Eds.), Isoscapes. Springer, Dordrecht, pp. 299–318. Available. https://doi.org/10.1007/978-90-481-3354-3_14.

Graustein, W.C., Armstrong, R.L., 1983. The use of strontium-87/strontium-86 ratios to measure transport into forested watersheds. Science 219, 289–292. https://doi.org/10.1126/science.219.4582.289.

Grupe, G., Price, T.D., Schröter, Söllner, F., Johnson, C.M., Beard, B.L., 1997. Mobility of bell beaker people revealed by strontium isotope ratios of tooth and bone: a study of southern Bavarian skeletal remains. Appl. Geochem. 12, 517–525. https://doi.org/10.1016/S0883-2927(97)00030-9.

Hartman, G., Richards, M., 2014. Mapping and defining sources of variability in bioavailable strontium isotope ratios in the eastern Mediterranean. Geochim. Cosmochim. Acta 126, 250–264. https://doi.org/10.1016/j.gca.2013.11.015.

Hartmann, J., Moosdorf, N., 2012. The new global lithological map database GLiM: a representation of rock properties at the earth surface. Geochem Geophys Geosystems. 13, Q12004. https://doi.org/10.1029/2012GC004370.

Hobson, K.A., Barnett-Johnson, R., Cerling, T., 2010. Using isoscapes to track animal migration. In: West, J., Bowen, G., Dawson, T., Tu, K. (Eds.), Isoscapes. Springer, Dordrecht, pp. 273–298.

Holt, E., Perra, M., 2021. Progetto Pran'e Siddi: preliminary report of excavations at Nuraghe Sa Conca ' e sa Cresia (Siddi SU). Layers Archeol Territ Contesti. 6, 49–74. https://doi.org/10.13125/2532-0289/4608.

Holt, E., Evans, J.A., Madgwick, R., 2021. Strontium (87Sr/86Sr) mapping: a critical review of methods and approaches. Earth Sci. Rev. 216, 103593. https://doi.org/10.1016/j.earscirev.2021.103593.

Holt, E., Aguilar, J., Schirru, D., 2022. The early Nuragic settlement system of the Siddi plateau, south-central Sardinia. Quad. Della Soprintend. Archeol. Prov. Cagliari E Oristano 33, 79–104.

Janzen, A., Bataille, C.P., Copeland, S.R., Quinn, R.L., Ambrose, S.H., Reed, D., et al., 2020. Spatial variation in bioavailable strontium isotope ratios (87Sr/86Sr) in Kenya and northern Tanzania: implications for ecology, paleoanthropology, and archaeology. Palaeogeogr. Palaeoclimatol. Palaeoecol. 560, 109957. https://doi.org/10.1016/j.palaeo.2020.109957.

Johnson, L.J., 2018. Finding Radiogenic Sr-Isotope Biospheres: Can a Home in Britain Be Found for People with High 87Sr/86Sr? PhD Dissertation. Durham University. Available. http://etheses.dur.ac.uk/12637/.

Käßner, A., Kalapurakkal, H.T., Huber, B., Tichomirowa, M., 2023. A new water-based 87Sr/86Sr isoscape map of central and NE Germany, with special emphasis on mountainous regions. Aquat. Geochem. 29, 95–125. https://doi.org/10.1007/s10498-023-09412-5.

Kramer, R.T., Kinaston, R.L., Holder, P.W., Armstrong, K.F., King, C.L., Sipple, W.D.K., et al., 2022. A bioavailable strontium (87Sr/86Sr) isoscape for Aotearoa New Zealand: implications for food forensics and biosecurity. PLoS One 17, e0264458. https://doi.org/10.1371/journal.pone.0264458.

Laffoon, J.E., Sonnemann, T.F., Shafie, T., Hofman, C.L., Brandes, U., Davies, G.R., 2017. Investigating human geographic origins using dual-isotope (87Sr/86Sr, δ18O) assignment approaches. PLoS One 12, e0172562. https://doi.org/10.1371/journal.pone.0172562.

Lahtinen, M., Arppe, L., Nowell, G., 2021. Source of strontium in archaeological mobility studies—marine diet contribution to the isotopic composition. Archaeol. Anthropol. Sci. 13, 1. https://doi.org/10.1007/s12520-020-01240-w.

Lai, L., Fonzo, O., Tykot, R.H., Goddard, E., Hollander, D., 2011. Le due comunità di Scaba 'e Arriu (Siddi). Risorse alimentari nella Sardegna del III millennio a.C. indagate tramite analisi isotopiche di tessuti ossei. Studio antropologico dei reperti umani. In: Atti della XLIII Riunione Scientifica Istituto Italiano di Preistoria e Protostoria, Bologna (Italy), 26–29 novembre 2008 L'età del rame in Italia. Istituto Italiano di Preistoria e Protostoria, Firenze, pp. 401–408.

Lai, L., Fonzo, O., Pacciani, E., O'Connell, T., 2014. Isotopi Stabili e Radioattivi: Primi Dati su Dieta e Cronologia Assoluta delle Sepolture di Monte'e Prama. In: Minoja, M., Usai, A. (Eds.), Le sculture di Mont'e Prama Contesto, scavi e materiali. Gangemi Editore, Roma, pp. 207–218.

Lai, L., Fonzo, O., O'Connell, T., 2017. L'Allevamento del Bestiame Presso il Nuraghe Arrubiu di Orroli: Primi Dati Isotopici dal Collagene. In: Perra, M., Lo Schiavo, F. (Eds.), Il Nuraghe Arrubiu di Orroli Volume 1 La Torre Centrale e il Cortile B: Il Cuore del Gigante Rosso. Arkadia Editore, Cagliari, pp. 123–127.

Lazzerini, N., Balter, V., Coulon, A., Tacail, T., Marchina, C., Lemoine, et al., 2021. Monthly mobility inferred from isoscapes and laser ablation strontium isotope ratios in caprine tooth enamel. Sci. Rep. 11, 2277. https://doi.org/10.1038/s41598-021-81923-z.

Liaw, A., Wiener, M., 2002. Classification and regression by randomForest. R News. 2, 18–22.

Lugli, F., Cipriani, A., Bruno, L., Ronchetti, F., Cavazzuti, C., Benazzi, S., 2022. A strontium isoscape of Italy for provenance studies. Chem. Geol. 587, 120624–1–10. https://doi.org/10.1016/j.chemgeo.2021.120624.

Lykoudis, S.P., Argiriou, A.A., 2007. Gridded data set of the stable isotopic composition of precipitation over the eastern and central Mediterranean. J. Geophys. Res. Atmospheres. 112 (D18107). https://doi.org/10.1029/2007JD008472.

Madgwick, R., Lamb, A.L., Sloane, H., Nederbragt, A.J., Albarella, U., Parker Pearson, M., et al., 2019. Multi-isotope analysis reveals that feasts in the Stonehenge environs and across Wessex drew people and animals from throughout Britain. Sci. Adv. 5, 1–12. https://doi.org/10.1126/sciadv.aau6078 eaau6078.

Madgwick, R., Lamb, A., Sloane, H., Nederbragt, A., Albarella, U., Parker Pearson, M., et al., 2021. A veritable confusion: use and abuse of isotope analysis in archaeology. Archaeol. J. 178, 361–385. https://doi.org/10.1080/00665983.2021.1911099.

Maurer, A.-F., Galer, S.J.G., Knipper, C., Beierlein, L., Nunn, E.V., Peters, D., et al., 2012. Bioavailable 87Sr/86Sr in different environmental samples — effects of anthropogenic contamination and implications for isoscapes in past migration studies. Sci. Total Environ. 433, 216–229. https://doi.org/10.1016/j.scitotenv.2012.06.046.

Nier, A.O., 1938. Isotopic constitution of Sr, Ba, bi, Ti, and hg. Phys. Rev. 54, 275–278. https://doi.org/10.1103/PhysRev.54.275.

Potter, P., Ramankutty, N., Bennett, E.M., Donner, S.D., 2010. Characterizing the spatial patterns of global fertilizer application and manure production. Earth Interact. 14, 1–22. https://doi.org/10.1175/2009EI288.1.

Potter, P., Ramankutty, N., Bennett, E.M., Donner, S.D., 2012. Global Fertilizer and Manure, Version 1: Phosphorus Fertilizer Application. NASA Socioeconomic Data and Applications Center (SEDAC), Palisades, New York. https://doi.org/10.7927/H4FQ9TJR.

Price, T.D., Johnson, C.M., Ezzo, J.A., Ericson, J., Burton, J.H., 1994. Residential mobility in the prehistoric Southwest United States: a preliminary study using strontium isotope analysis. J. Archaeol. Sci. 21, 315–330. https://doi.org/10.1006/jasc.1994.1031.

Reich, M.S., Flockhart, D.T.T., Norris, D.R., Hu, L., Bataille, C.P., 2021. Continuous-surface geographic assignment of migratory animals using strontium isotopes: a case study with monarch butterflies. Methods Ecol. Evol. 12, 2445–2457. https://doi.org/10.1111/2041-210X.13707.

Rogers, K.M., Wassenaar, L.I., Soto, D.X., Bartle, J.A., 2012. A feather-precipitation hydrogen isoscape model for New Zealand: implications for eco-forensics. Ecosphere 3, 1–13. https://doi.org/10.1890/ES11-00343.1.

Romaniello, S.J., Field, M.P., Smith, H.B., Gordon, G.W., Kim, M.H., Anbar, A.D., 2015. Fully automated chromatographic purification of Sr and ca for isotopic analysis. J. Anal. At. Spectrom. 30, 1906–1912. https://doi.org/10.1039/C5JA00205B.

Ryan, S., Snoeck, C., Crowley, Q.G., Babechuk, M.G., 2018. 87Sr/86Sr and trace element mapping of geosphere-hydrosphere-biosphere interactions: a case study in Ireland. Appl. Geochem. 92, 209–224. https://doi.org/10.1016/j.apgeochem.2018.01.007.

Scaffidi, B.K., Tung, T.A., Gordon, G.W., Alaica, A.K., González La Rosa, L.M., Marsteller, S.J., et al., 2020. Drinking locally: a water 87Sr/86Sr Isoscape for geolocation of archeological samples in the Peruvian Andes. Front. Ecol. Evol. 8, 281. https://doi.org/10.3389/fevo.2020.00281.

Sealy, J.C., van der Merwe, N.J., Hobson, K.A., Horton, D.R., Lewis, R.B., Parkington, J., et al., 1986. Isotope assessment and the seasonal- mobility hypothesis in the southwestern cape of South Africa [and comments and replies]. Curr. Anthropol. 27, 135–144. https://doi.org/10.1086/203404.

Serna, A., Prates, L., Mange, E., Salazar-García, D.C., Bataille, C.P., 2020. Implications for paleomobility studies of the effects of quaternary volcanism on bioavailable strontium: a test case in North Patagonia (Argentina). J. Archaeol. Sci. 121, 105198. https://doi.org/10.1016/j.jas.2020.105198.

Sillen, A., Hall, G., Richardson, S., Armstrong, R., 1998. 87Sr/86Sr ratios in modern and fossil food-webs of the Sterkfontein Valley: implications for early hominid habitat preference. Geochim. Cosmochim. Acta 62, 2463–2473. https://doi.org/10.1016/S0016-7037(98)00182-3.

Tarrant, D., Hepburn, J., Renson, V., Richards, M., 2024. A pilot bioavailable strontium isotope baseline map of southern British Columbia, Canada. Facets 9, 1–11. https://doi.org/10.1139/facets-2023-0173.

Thomsen, E., Andreasen, R., 2019. Agricultural lime disturbs natural strontium isotope variations: implications for provenance and migration studies. Sci. Adv. 5, eaav8083. https://doi.org/10.1126/sciadv.aav8083.

Thomsen, E., Andreasen, R., Rasmussen, T.L., 2021. Homogeneous glacial landscapes can have high local variability of strontium isotope signatures: implications for prehistoric migration studies. Front. Ecol. Evol. 8, 588318. https://doi.org/10.3389/fevo.2020.588318.

Trueman, C.N., MacKenzie, K.M., Palmer, M.R., 2012. Identifying migrations in marine fishes through stable-isotope analysis. J. Fish Biol. 81, 826–847. https://doi.org/10.1111/j.1095-8649.2012.03361.x.

van der Veer, G., Voerkelius, S., Lorentz, G., Heiss, G., Hoogewerff, J.A., 2009. Spatial interpolation of the deuterium and oxygen-18 composition of global precipitation using temperature as ancillary variable. J. Geochem. Explor. 101, 175–184. https://doi.org/10.1016/j.gexplo.2008.06.008.

Wang, X., Bocksberger, G., Lautenschläger, T., Finckh, M., Meller, P., O'Malley, G.E., et al., 2023. A bioavailable strontium isoscape of Angola with implications for the archaeology of the transatlantic slave trade. J. Archaeol. Sci. 154, 105775. https://doi.org/10.1016/j.jas.2023.105775.

Weber, M., Lugli, F., Jochum, K.P., Cipriani, A., Scholz, D., 2018. Calcium carbonate and phosphate reference materials for monitoring bulk and microanalytical determination of Sr isotopes. Geostand. Geoanal. Res. 42, 77–89. https://doi.org/10.1111/ggr.12191.

Willmes, M., Bataille, C.P., James, H.F., Moffat, I., McMorrow, L., Kinsley, L., et al., 2018. Mapping of bioavailable strontium isotope ratios in France for archaeological provenance studies. Appl. Geochem. 90, 75–86. https://doi.org/10.1016/j.apgeochem.2017.12.025.

Wright, M.N., Ziegler, A., 2017. Ranger: a fast implementation of random forests for high dimensional data in C++ and R. J. Stat. Softw. 77, 1–17. https://doi.org/10.18637/jss.v077.i01.

Zieliński, M., Dopieralska, J., Belka, Z., Walczak, A., Siepak, M., Jakubowicz, M., 2016. Sr isotope tracing of multiple water sources in a complex river system, Noteć River, Central Poland. Sci. Total Environ. 307–316. https://doi.org/10.1016/j.scitotenv.2016.01.036.

Zieliński, M., Dopieralska, J., Królikowska-Ciągło, S., Walczak, A., Belka, Z., 2021. Mapping of spatial variations in Sr isotope signatures (87Sr/86Sr) in Poland — implications of anthropogenic Sr contamination for archaeological provenance and migration research. Sci. Total Environ. 775, 145792. https://doi.org/10.1016/j.scitotenv.2021.145792.